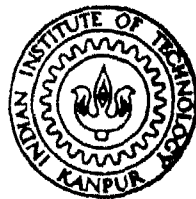


# **LOW TEMPERATURE MACHINING OF MILD STEEL AND TITANIUM**

by  
**RAJINDER JEET SINGH BAGGA**



**DEPARTMENT OF MECHANICAL ENGINEERING**  
**INDIAN INSTITUTE OF TECHNOLOGY, KANPUR**  
MAY, 1987

# **LOW TEMPERATURE MACHINING OF MILD STEEL AND TITANIUM**

A Thesis Submitted  
In Partial Fulfilment of the Requirements  
for the Degree of

**MASTER OF TECHNOLOGY**

by

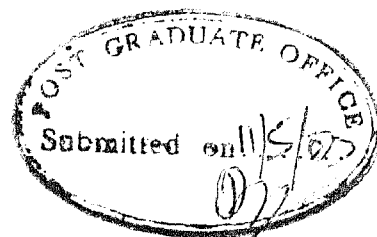
**RAJINDER JEET SINGH BAGGA**

to the

**DEPARTMENT OF MECHANICAL ENGINEERING**



**INDIAN INSTITUTE OF TECHNOLOGY, KANPUR**

**MAY, 1987.**



## CERTIFICATE

This is to certify that the present work entitled, "LOW TEMPERATURE MACHINING OF MILD STEEL AND TITANIUM", has been carried out under our supervision and has not been submitted elsewhere for the award of a degree.

	
(A. Ghosh)	(M.K. Muju)
Professor	Professor
Department of Mechanical Engineering	
Indian Institute of Technology, Kanpur	
INDIA	

May, 1987.

## ABSTRACT

Materials having high strength and low thermal conductivity are being used increasingly. Despite advance in cutting tool materials, considerable difficulties are experienced while machining materials with low thermal conductivity. Due to enormous temperature rise tool wear becomes main problem. In many cases conventional cutting fluid becomes ineffective. In first part of ~~work~~ the present work machining of mild steel at low temperature has been investigated. Liquid Nitrogen was used to cool work piece prior to machining.

A study has been made about the effect of low temperature on cutting forces, coefficient of friction mechanism of chip formation while cutting with high speed tool. It has been established that with the increase in cooling the cutting forces reduces and chip ratio increases and coefficient of friction increase.

In second part of the work machining of commercially pure titanium was conducted. The effect of liquid nitrogen on the cutting forces, tool-chip interface temperature and chip formation have been investigated. It is found that the percentage drop in temperature is more when machining Titanium than when machining mild steel but reduction in cutting force is less than with mild steel. Increase in productivity at low temperature for some wear as that in dry cutting has been reported.

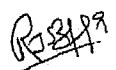
ACKNOWLEDGEMENTS

I wish to record my deep sense of gratitude and appreciation to my thesis supervisors, Professor M.K. Muju and Professor A. Ghosh for suggesting the problem and valuable guidance throughout the programme. Their generous attitude towards academic liberty has been a source of inspiration for me.

I wish to express my heartfelt gratitude to Mr. R.M. Jha, Mr. B.P. Bhartiya, Mr. H.P. Sharma, Sri O.P. Bajaj and Mr. Panna Lal of Mechanical Engineering Department for their cooperation and guidance, which they rendered so willingly during the course of experiments. I deeply appreciate help from Mr. P.N. Mishra of Refrigeration and Airconditioning Laboratory and Mr. Mukherjee (Dada) of Physical Metallurgical Laboratory. I am also thankful to all staff of Liquid Nitrogen Plant for providing liquid nitrogen on odd times.

I deeply acknowledge my friends Mr. Alesu, Mr. Bharat Bhushan, Mr. Bhagirath Gohil, Mr. Jaydeep Ghosh and Mr. R. Nakalil for their help and valuable suggestions. I highly value the association with my friends Mr. G.K. Adil, Mr. Manoj Kumar Jain, Mr. Parmod Pandey, Mr. Majumdar, Mr. Ajay Singh, Mr. Pankaj Arora and Mr. Shailesh Singh and others with whom I shared my ideas.

Finally, I wish to thank Mr. U.S. Misra for the good typing and Mr. B.K. Jain for his neat tracing.

  
-RAJINDER JEET SINGH BAGGA

## CONTENTS

	<u>Page</u>
CHAPTER 1 INTRODUCTION	1
1.1 Introduction	1
1.2 Properties of Materials at Low Temperature	2
1.2.1 Tensile Properties	3
1.2.2 Thermal Properties	6
(a) Specific Heat	6
(b) Thermal Conductivity	7
1.2.3 Mechanical Properties of Some Engineering Alloys	12
(a) Iron Base Alloy	12
(b) Nickel and Cobalt Base Alloys	13
(c) Titanium Base and Titanium Base Alloy	15
1.3 Mechanism of Chip Formation and Type of Chips	16
1.3.1 Mechanism	16
1.3.2 Principal Chips Types	18
(a) Discontinuous Chips	18
(b) Continuous Chips	20
(c) Continuous Chips with BUE	21
1.4 Previous Research	21
1.4.1 Cutting at Low Temperature	21
1.4.2 Machining of Titanium Alloys and Formation of Serrated Chips	25
1.5 Objective and Scope of Present Work	34
CHAPTER 2 MACHINING IN LIQUID NITROGEN ENVIRONMENT	36
2.1 Introduction	36
2.2 Experimental Setup	36
2.2.1 Experimental Setup for Cooling Arrangement	38
2.2.2 Experimental Setup for Force Measurement	42
2.2.3 Experimental Set-up for Temperature Measurement	42
2.3 Tool Material	48
2.4 Work Material	49
2.5 Experimental Procedure	50
CHAPTER 3 RESULT AND DISCUSSIONS	53
3.1 Machining of Mild Steel	53
3.1.1 Cutting Temperature	53
3.1.2 Cutting Forces	57
3.1.3 Calculation of Maximum Tool-Chip Interface Temperature	67

	<u>Page</u>
3.2 Machining of Titanium	85
3.2.1 Cutting Temperature	85
3.2.2 Cutting Force	90
3.2.3 Improvement in Wear	95
CHAPTER 4 CONCLUSIONS AND SCOPE OF FURTHER RESEARCH	98
4.1 Conclusion	98
4.2 Scope of Further Research	99
REFERENCES	100

LIST OF TABLES

<u>Table No.</u>	<u>Title</u>	<u>Page</u>
3.1	Comparison of shear plane angle $\phi$ and $\phi_{EM}$ feed = .05mm/rev.	59-60
3.2	Comparison of shear plane angle $\phi$ and $\phi_{EM}$ feed = .125 mm/rev.	61-62
3.3	Comparison of (theoretical and experimental) cutting force ratio using only one nozzle	68
3.4	Comparison of (theoretical and experimental) cutting force ratio using only two nozzle	69
3.5	Comparison of (theoretical and experimental) cutting force ratio using only four nozzle	70
3.6	Comparison of (theoretical and experimental) tool-chip interface temperature when machining MS in dry condition	77
3.7	Comparison of (theoretical and experimental) tool-chip interface temperature when machining MS in using only one nozzle.	78
3.8	Comparison of (theoretical and experimental) tool-chip interface temperature when cutting MS with two nozzles .	79
3.9	Comparison of (theoretical and experimental) tool-chip interface temperature when machining MS using only four nozzles	80



<u>Table No.</u>	<u>Title</u>	<u>Page</u>
3.10	Comparison of (theoretical and experimental) tool-chip interface temperature when machining Titanium	89
3.11	Comparison of specific cutting energy	93
3.12	Comparison of (theoretical and experimental) force ratio when cutting Titanium using four nozzles	94

# LIST OF FIGURES

<u>Figure No.</u>	<u>Title</u>	<u>Page</u>
1.1	Temperature variation of elastic constants for six metals	5
1.2	Specific heat as a function of temperature	8
1.3	Heat transport mechanism	10
1.4	Thermal conductivity and thermal diffusivity as a function of temperature	11
1.5	Yield and ultimate strength as a function of temperature for iron base alloys	14
1.6	Yield strength as a function of temperature for Titanium alloys	17
1.7	Formation of different types of chips	19
1.8	AJM of glass at low temperature	26
1.9	Schematic diagram of a sequence of events, showing various stages involved in chip formation when machining Titanium alloys	29
1.10	Sequence of events during the formation of one chip segment presented together with complementary force and temperature profile	32
1.11	Energy partition in machining of Ti alloys	33
2.1	Variation of wear land (w) with cutting time $T_c$ for different cutting fluids	37
2.2	Schematic diagram for cooling arrangement	39
2.3	Holding device for nozzle in position	41

<u>Figure No.</u>	<u>Title</u>	<u>Page</u>
2.4	Dynamometer calibration curve input voltage = 7 volts	43
2.5	Schematic diagram for measuring chip- tool interface temperature	45
2.6	Arrangement for calibration of tool work thermocouple	46
2.7	Temperature calibration curve for mild steel and Titanium with HSS	47
3.1	Variation of interface temperature with speed (experimental) feed = .05 mm/rev	54
3.2	Variation of interface temperature with speed (experimental) feed = .125 mm/rev	55
3.3	Range of % fall in temperature with mass flow rate of liquid nitrogen	56
3.4	Variation of percentage drop in interface temperature with speed, feed = .125 mm/rev	58
3.5	Variation of cutting force with speed (experimental) feed = .05 mm/rev	63
3.6	Variation of cutting force with feed (experimental) feed = .125 mm/rev	64
3.7	Variation of mean coefficient of friction ( $\mu$ ) with speed (experimental) feed = .05 mm/ rev	66
3.8	Comparison of (theoretical and experimental) cutting force ratio	71

<u>Figure No.</u>	<u>Title</u>	<u>Page</u>
3.9	Comparison of (theoretical and experimental) maximum tool-chip interface temperature	81
3.10	Variation of heat partitioning factor with cutting condition	83
3.11	Effect of $\rho_{ct} V \tan \phi / K$ on division of shear heat between chip and workpiece where $\lambda =$ the proportion of shear zone heat conducted to workpiece	84
3.12	Variation of <sup>interface</sup> cutting temperature with speed (experimental) feed = .05 mm/rev	86
3.13	Variation of interface temperature with speed, feed = .125 mm/rev	87
3.14	Percentage variation in temperature with speed, feed = .05 mm/rev	88
3.15	Variation of cutting forces with speed (experimental), feed = .05 mm/rev	91
3.16	Variation of cutting force with speed (experimental), feed = .125 mm/rev	92
3.17	Variation of percentage gain factor G speed (experimental) for Titanium	97

## NOMENCLATURE

$b$	width of cut
$c$	specific heat
$F$	friction force
$F_c$	cutting force
$F_t$	thrust or <del>fix</del> <sup>e</sup> ed force
$k$	thermal conductivity
$l$	length of contact between chip and tool
$N$	normal load
$r$	cutting ratio, chip thickness ratio
$t_1$	uncut chip thickness or feed
$t_2$	cut chip thickness
$U_c$	specific energy
$V$	cutting velocity
$W_o$	rate of heat generation in primary deformation zone
$W_s$	rate of heat generation in secondary deformation zone
$\rho$	density of the material
$\theta_p$	temperature rise in primary deformation zone
$\theta_s$	temperature rise in secondary deformation zone
$\alpha$	side rake angle
$\phi$	shear angle
$\theta_o$	initial temperature of workpiece
$\theta_{total}$	maximum temperature rise
$\phi_{EM}$	shear angle calculated from Ernst, Marchant's theory
$\mu$	coefficient of friction between tool and chip
$\lambda$	fraction of primary heat which goes to workpiece
	thermal number
$\beta$	friction angle

## CHAPTER 1

### INTRODUCTION

#### 1.1 Introduction

Machining under room temperature conditions is the most convenient and is still the most common process of producing components. But, irrespective of the possibility that new methods of machining may prove industrially practical, the attempted development of a new method may serve two usual purposes. First, we may learn from the new method the characteristics hitherto unknown or unsuspected principles or patterns of behaviour may be evident. Secondly, we may develop by this liberal approach newer methods of machining which may have advantage over current ones.

Temperature rise during the cutting not only reduces the tool life but also impairs the product quality by chemical action and induction of residual tensile stress as also microcracks at the machined surface. This problem is acute when the cutting speed is high and work material is heat resistant or difficult to machine. The harmful effects of high machining temperatures may be substantially controlled by adopting the following strategic principles:

1. By controlling the quantity of heat generated by improving the machinability criteria of the work and tool and

by optimizing the process parameters.

2. By removing the heat from cutting zone with a coolant.

3. By reducing the effect of temperature particularly on the tool.

Development of hard, tough and wear resistant tool materials such as coated carbide, tough ceramics, UCON, BORZON have enhanced the cutting tool level to cope up with high temperature effects. The detrimental effect of high temperature on the work surface, however, are still a problem in high speed machining.

Profused cooling with conventional <sup>coolants</sup> cutting even in the form of jet or mist is virtually unable to solve this problem. Under such circumstances cryogenic cooling by agents like liquid nitrogen which is gradually being made available at lower cost, may meet the challenge offered by heat and its effects. Research has already been undertaken to explore the benefits of cryogenic machining to evaluate its economic feasibility.

## 1.2 Properties of Material at Low Temperature

Research in cryogenic engineering during the late 1800s led to the liquification of Oxygen (1871) following by Nitrogen (1883), Hydrogen (1891) and finally Helium (1908). These fluids provided scientists, the opportunity to conduct research at low temperatures. In the following section properties of material

which are expected to influence the machining behaviour of metal have been discussed.

### 1.2.1 Tensile Properties

High temperature means higher order of thermal vibration of atoms and diffusion and vice versa. Deformation in solid is only due to stepwise movement of dislocations through a lattice. There always exist a stress barrier surrounding the dislocation which resist the motion of involved atoms [1]. The deformation properties at low temperature are changed because there is less thermal activation available to assist the dislocation to overcome the obstacles. In the absence of thermal activation more force is required to overcome the force barriers. As a result at low temperature yield and tensile strength usually increases. Generally higher stresses are required to develop equivalent amount of strains.

This dislocation theory is verified by different behavior of yield strength of fcc and bcc lattices. Yield strength of fcc materials increases by 20 to 30% while yield strength of the bcc material increases by 100% [2]. In this case it is clear that behaviour of bcc materials is more temperature dependent. fcc materials retain their ductility at low temperature but bcc materials become brittle [3]. These are characterized by a ductile-brittle transition region which occurs over a narrow range. Below transition temperature, the metal breaks in a brittle fashion with little or no plastic



deformation. At low temperature thermal activation will not be so effective in helping the dislocation to pull away from their impurity atmospheres and yield stress increases. The reason why this effect is not observed in fcc metal is given as, in fcc structure an impurity atom produces a spherically symmetrical distortion of the lattice and it is only attracted to the edge dislocation. The screw dislocation are left free of impurity, and thus can move under a much lower stress. In bcc materials the impurity atoms cause a nonspherical distortion of the lattice and some of this strain can be relieved by the screw dislocation as well. Thus all the dislocation can be anchored by the impurity atoms. Characteristics of hcp materials fall between fcc and bcc alloys. In many case it behaves more likely bcc alloys [12].

Several theories have been also given to explain the change of tensile properties of materials at low temperature [2].

Elastic properties of crystal is affected by lattice vibration. Elastic properties of crystal are determined primarily by strain dependence of harmonic frequency distribution of the crystal lattice. Frequency of vibration of crystalline prism can be determined with the help of elastic constants.

Elastic constants are physical properties relating stress to strain. Figure 1.1 show how various elastic constants vary with temperature between 0°K and 300°K. Elastic stiffness of material increases by 5 to 15% during cooling.

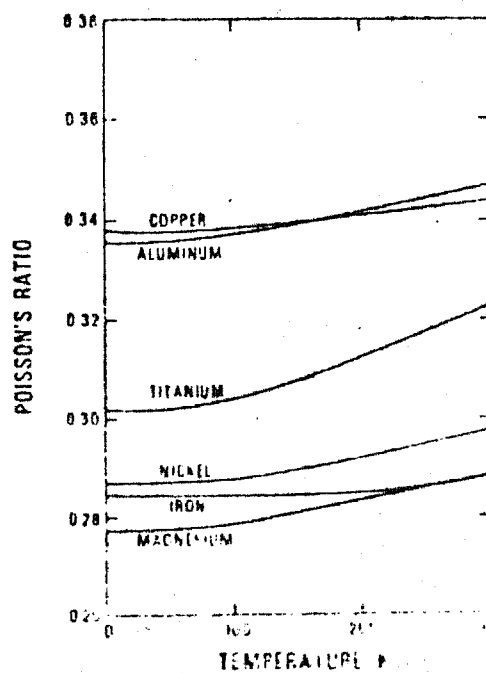
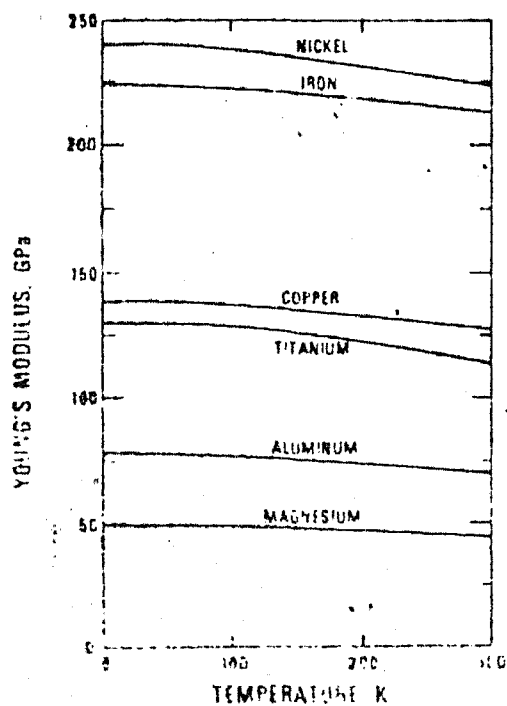
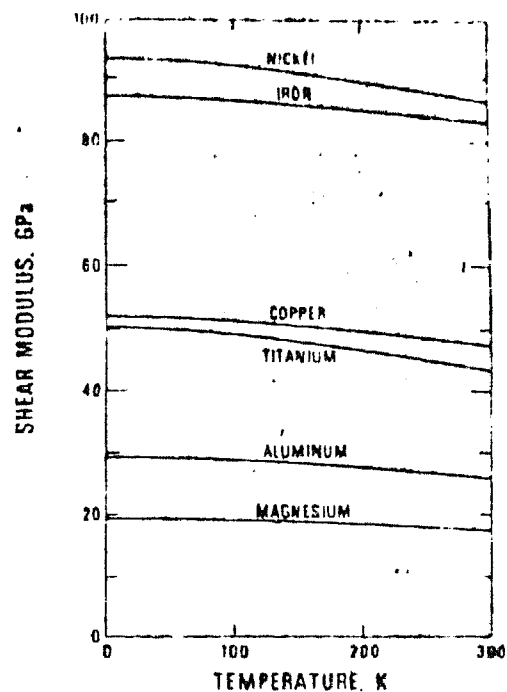
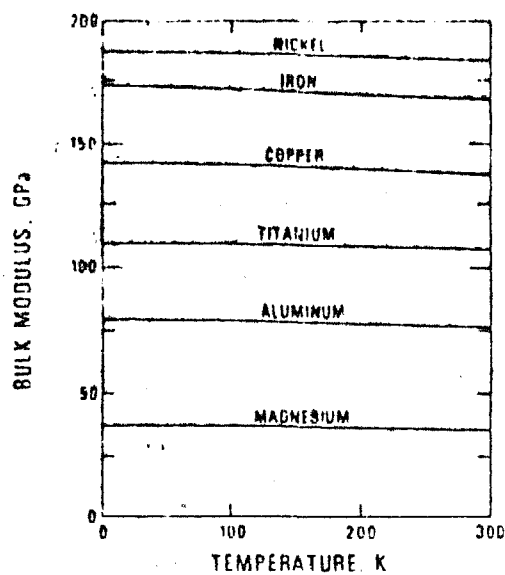


FIG. 1-1 TEMPERATURE VARIATION OF ELASTIC CONSTANTS FOR SIX METALS[10].

### 1.2.2 Thermal Properties

Thermal properties of materials determine the relative rate of temperature rise at the tool edge, the ultimate distribution of heat between tool chip and workpiece and the probability of incurring residual stress in the part due to thermal growth and plastic flow.

#### (a) Specific Heat

Heat capacity  $c$  defined as the amount of heat required to raise the temperature of a system by a unit of temperature

$$c = \frac{dQ}{dT}$$

The heat capacity per unit mass is called the specific heat.

Before the advent of the quantum theory the value of specific heats of solids were calculated using the classical theorem of equipartition<sup>of</sup> energy. It was assumed that, each atom or molecule in a solid is able to vibrate about a fixed point. This vibration can extend in three dimensions. Equipartition of energy theorem ascribes an energy of  $3KT$  to each atom or molecule. From this assumption molar specific heat has the constant value  $3R = 29.94 \text{ J mol}^{-1} \text{ deg}^{-1}$ . This relationship is very successful both at and above room temperatures, but fails to determine the specific heat at low temperatures. Einstein (1907) and later Debey tried to explain decrease in specific heat at low temperature.

According to Debey theory atomic system is assumed to be an elastic continuum in which only certain frequency can be excited and maintained. These will be those which are able to set-up standing waves in the medium, any others will die out rapidly [4]. Debey assumed lattice vibrate with a upper limit to the vibrational frequencies. He developed a formula which co-relate the specific heat with  $T^3$  at low temperatures

$$C_v = 1944 r \left( \frac{T}{\theta_D} \right)^3 \text{ J mol}^{-1} \text{ K}^{-1}$$

$C_v$  = specific heat,

$\theta_D = h\nu/kT$

$r$  = number of atoms per molecule.

From the above discussion it is clear that specific heat is a strong function of temperature, particularly for  $T \leq 200^\circ\text{K}$ . Figure 1.2 shows the specific heat as a function of temperature for several types of material [5].

#### (b) Thermal Conductivity

Thermal donductivity correlates the two parameters, heat flow and temperature gradient. For steady state unidirectional heat flow through an isotropic medium, this relationship is given by the equation:

$$\frac{Q}{A} = -K \frac{dT}{dx}$$

$Q$  - Rate of heat flow,

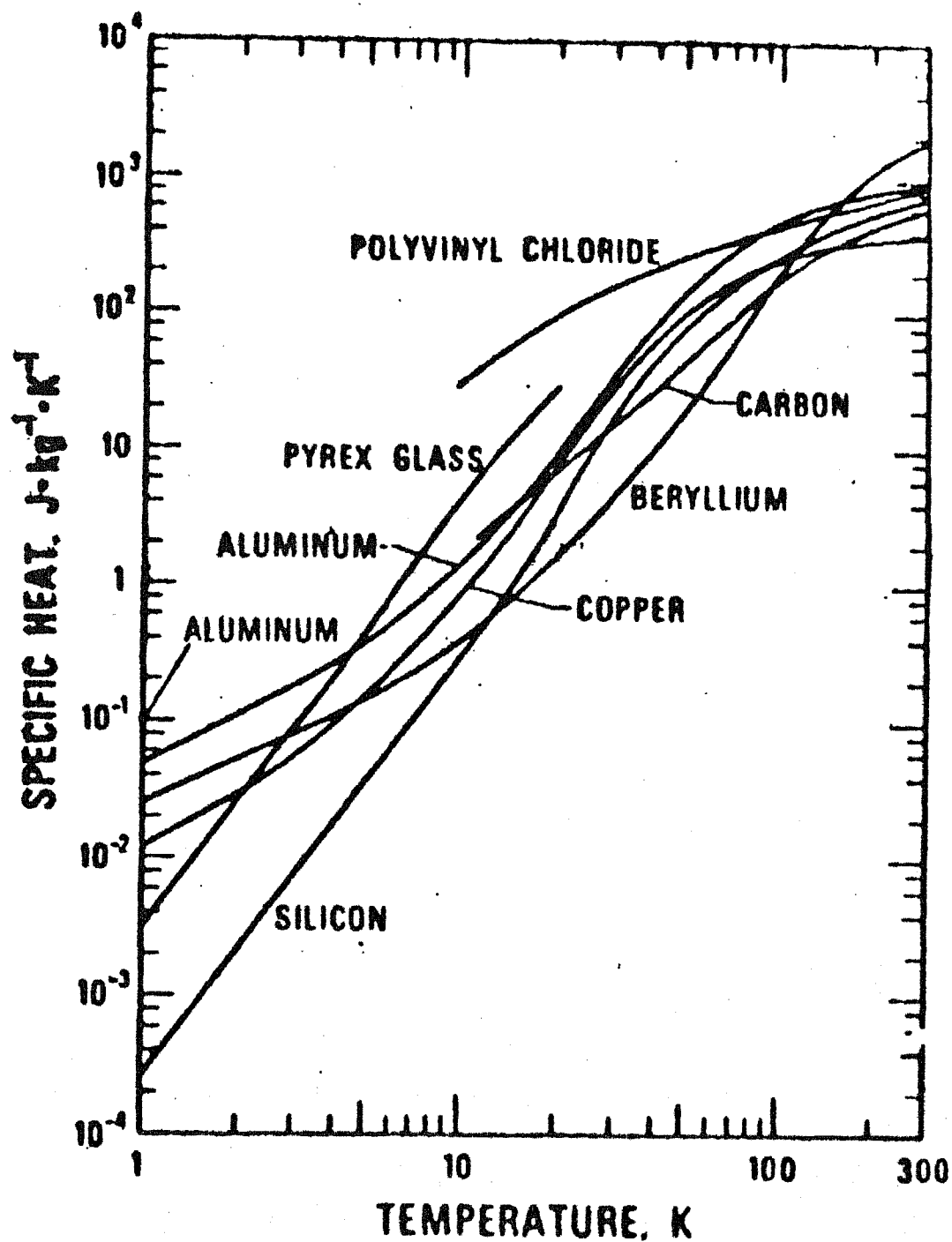


FIG. 1.2: SPECIFIC HEAT AS A FUNCTION OF TEMPERATURE [10].

A - Area through which heat is passing,

K - constant of proportionality known as thermal conductivity.

Different type of materials have different mode of conduction. In pure metal and dilute alloys the free electrons are solely responsible for conduction of heat. In case of highly alloyed metal the heat conducted by quantized lattice vibration (phonons) becomes more dominant. In non-metal and structural material the heat is conducted only by phonons and in semi-conductor material electron holes pair conduction is present. Figure 1.3 shows the heat conduction mechanism.

In metals while conducting heat, movement of free electron is generally restricted by phonons, lattice imperfection, other electrons and magnetic fields. Lattice vibration and lattice imperfection play most significant role in restricting the motion of electrons. Material imperfections become most important at low temperature [4]. Due to different types of crystal imperfection. Single value of conductivity can not be obtained at low temperature. Figure 1.4 gives an idea about the variation of thermal conductivity with change in temperature. As the temperature decreases, the alloy thermal conductivity decreases approximately linearly, whereas for the purer elements it is a complex dependency. For purer elements thermal conductivity reaches maximum then rapidly decreases as temperature approaches the absolute zero.

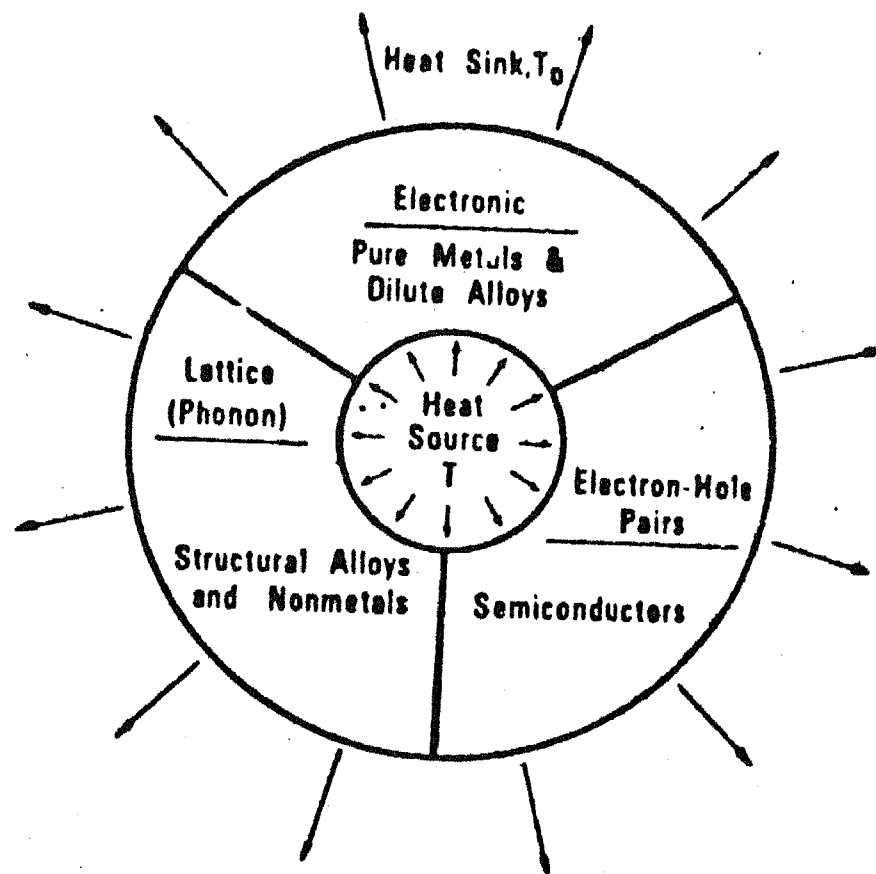


FIG. 1.3: HEAT TRANSPORT MECHANISM [10].

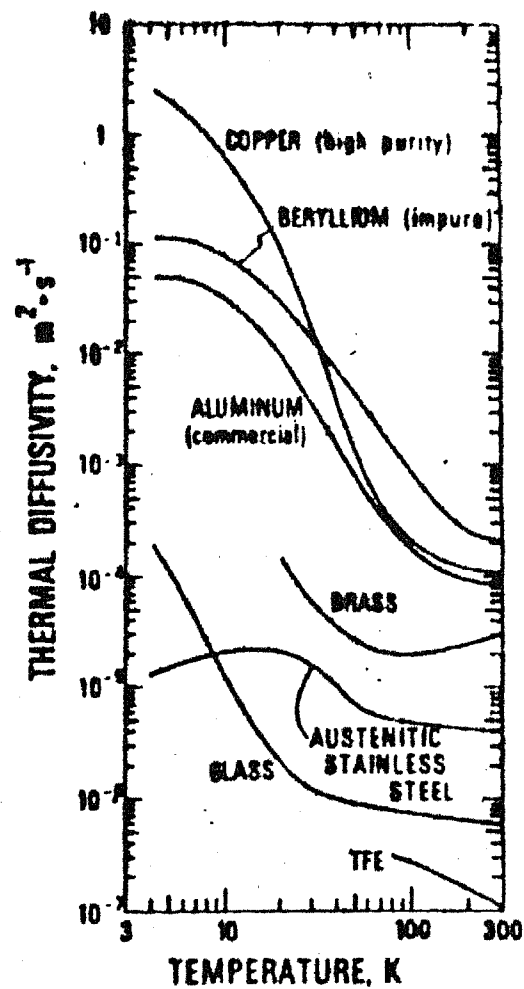
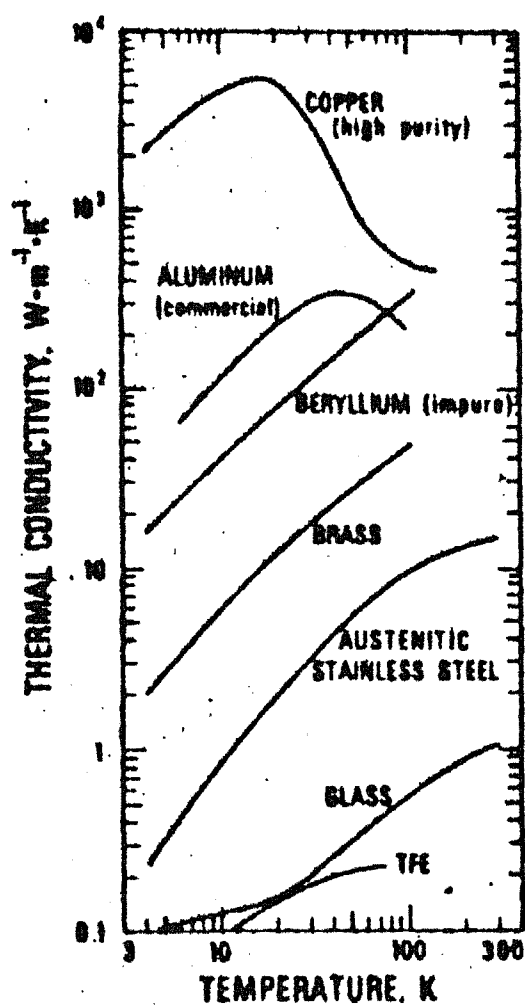


Fig 2.4 THERMAL CONDUCTIVITY AND THERMAL DIFFUSIVITY AS A FUNCTION OF TEMPERATURE [10].



### 1.2.3 Mechanical Properties of Some Engineering Alloys

It is important to remember that effect of cryogenic temperature on material is primarily dependent upon crystalline structure. The summarised review of typical effects for bcc, fcc, and hcp materials are given in Table 1.1. Temperature generally encountered in cryogenic testing are the boiling point of the liquified gases, e.g. 4°K (Helium), 20°K (Hydrogen), 77°K (Nitrogen), 90°K (Oxygen).

#### (a) Iron Base Alloys

At room and cryogenic temperature the Iron base alloys have either bcc or metastable fcc structures. Depending upon composition and microstructure of the material, the bcc base Iron alloys undergo a ductile to brittle transition in wide range of temperature varying from above room temperature to as low as 100-200°K. Reduction in temperature of pure <sup>iron</sup> ~~iron~~ causes large increase in yield and tensile strength, ultimate strength approaches the yield strength. Ductility and toughness are severely affected after transition temperature (100-150°K). After transition temperature, pure iron becomes brittle and shows zero ductility. Ingot and wrought iron have greater strength and lower ductility at room temperature, but behave quite similarly. Generally transition temperature is much higher and may even be room temperature depending upon the impurity and microstructure.

Low, medium and high carbon steel and cast iron possess a bcc structure and behave similarly as stated above. Transition temperature may vary over wide range from above room temperature to 150-200°K. Similarly high alloy ferritic and martensitic steel are affected much in the same way as carbon steel or low alloy steel and transition temperature range is from 150 to 300°K. Many of the austenitic stainless steels retain fcc structure from 298 to 4°K. Due to different type of crystal structure it behaves quite differently at cryogenic temperature than do the bcc iron alloy. At cryogenic temperature, large increases (100%) in tensile strength, smaller increase (20-50%) in yield strength and little or no effects on ductility have been found [2]. However, several of these steels have total or partial transformation from austenite to martensite. The properties of these type of materials are combination of fcc and bcc materials. Figure 1.5 summarize the effect of cryogenic temperature on the properties of base alloys.

(b) Nickel and Cobalt Base Alloy

The crystalline structure of nickel and cobalt are fcc and hcp respectively. However, nickel-cobalt alloy in which nickel is 10% possess fcc structure at room and cryogenic temperatures. At cryogenic temperature annealed nickel and cobalt alloys show increase in tensile strength by 100%, yield strength about 40-60%, [2]. Low temperature has no effect on its ductility and toughness. Aged and cold-rolled materials have increase of about 50% for both yield and tensile strength.

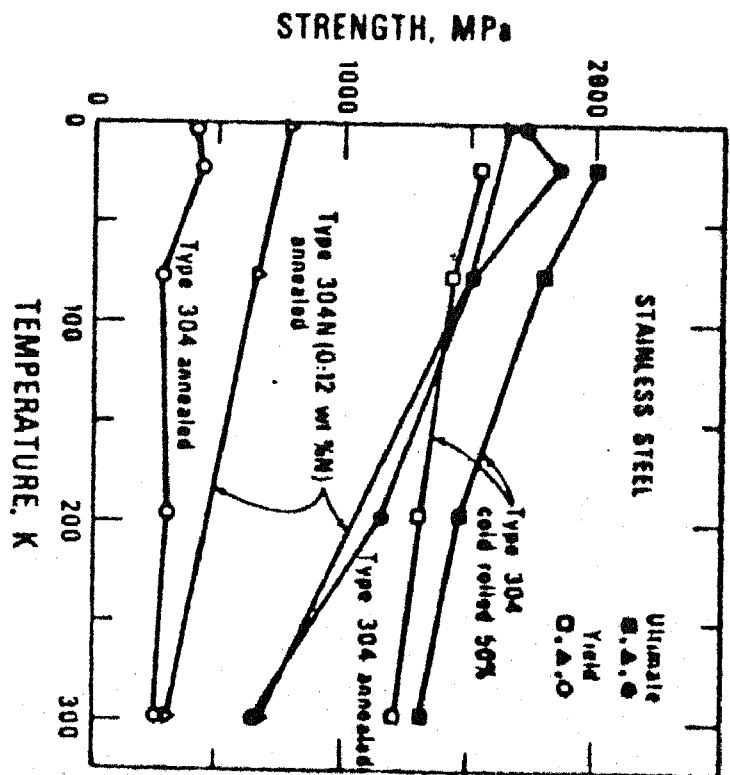
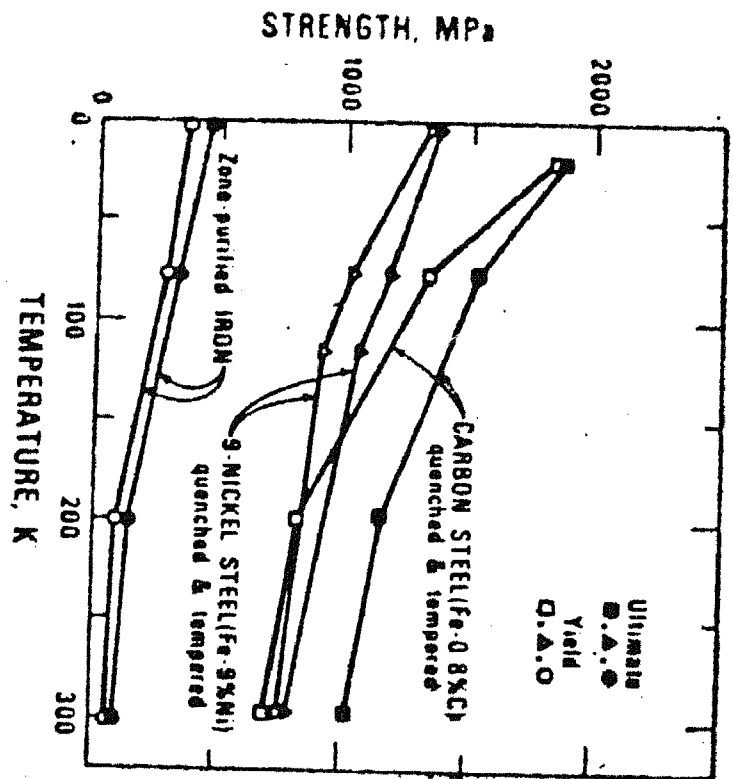


FIG. 2.65 YIELD AND ULTIMATE STRENGTHS AS A FUNCTION OF TEMPERATURE FOR IRON BASE ALLOYS [16].

(c) Titanium and Titanium Base Alloys

Structural titanium alloys are coming in for increased use because they are light, ductile and have good corrosion resistance. Some form of commercially pure Ti and some alloys show good cryogenic properties while high temperature properties are satisfactory. Titanium has a closed packed structure (alpha form) at temperature below  $885^{\circ}\text{C}$  and bcc (beta form) at higher temperatures. Addition of alloying elements changes the transformation temperature and also results in formation of solid solution and their metallic compounds. Depending on the crystalline structure, Titanium alloys fall into three classes: all alpha alloy; alpha beta alloys and all beta alloys.

Commercially pure Titanium and all alpha Titanium alloys have fairly low strength and are very ductile and tough at room temperature. Tensile and yield strength are greatly increased at cryogenic temperature. Due to presence of interstitial, ductility and toughness are greatly affected. But, very low interstitial grades of Titanium retain their ductility at low temperatures. Normal commercial amount of interstitials adversely affect the ductility of Titanium alloy. Toughness of Ti alloy decrease severely below temperature  $77^{\circ}\text{K}$ . The alpha-beta alloys are affected much in the same way as the alpha titanium alloys. However, most of alpha beta titanium alloys lose ductility and toughness at 200 to  $77^{\circ}\text{K}$ .

All beta Titanium alloys have very high strength and good weldability. Beta titanium behaves like bcc materials and becomes brittle at cryogenic temperature. Transition temperature for all  $\beta$ -Titanium alloy has been found to be at about 200°K.

The rate of increase of tensile strength of Titanium alloy exceeds the rate of increase of shear strength on reducing temperature. Figure 1.6 summarize the mechanical properties of Titanium alloys.

### 1.3 Mechanism of Chip Formation and Types of Chips

#### 1.3.1 Mechanism:

The action of cutting tool subjects the layer of metal being cut to compression. It is accompanied by elastic and plastic deformation. Plastic strain consists in the displacement of the metal in reference to other layers along the so-called slip planes which are considered to coincide with the direction of maximum shear strain. Such displacement occurs both between the particles of crystalline grain (in monocrystal) and between the grains themselves in a polycrystal. As a result of this displacement, the shape of grain, their size and relative position are changed. The process of plastic deformation is accompanied by much heat generation and change in the local properties of metal.

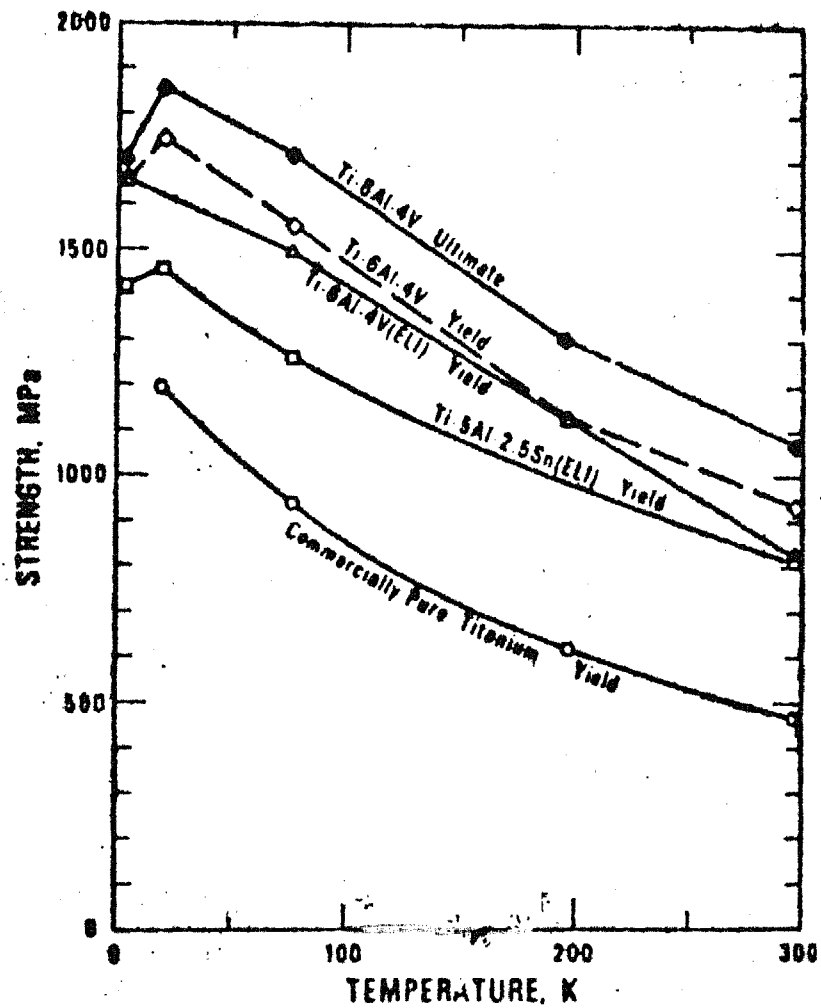


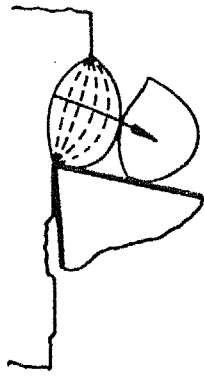
FIG. 1.16 YIELD STRENGTHS AS A FUNCTION OF TEMPERATURE FOR TITANIUM ALLOYS [10].

In metal cutting compression process differs from ordinary compression of a specimen loaded by surface approaching each other (platen of a testing machine) in that the layer being cut off is bound to the rest of the blank. Principal laws of ordinary compression are also valid for above compression, and that the chip forming process is actually the process of elastic plastic deformation of the layer being removed.

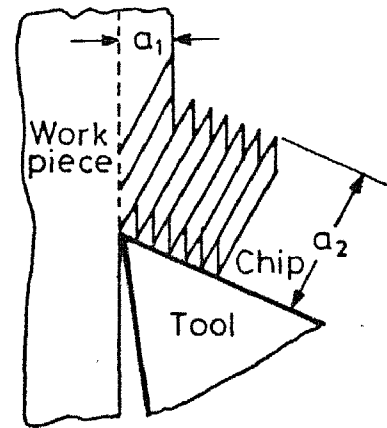
### 1.3.2 Principal Chip Types

#### (a) Discontinuous Chips

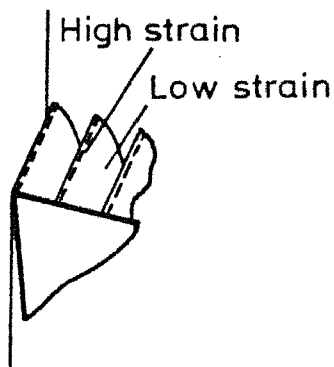
Discontinuous chips form where ~~(a)~~ cracks form periodically along a line of maximum shear stress (Fig. 1.7(a)). Between the cracks the material is extruded into region of highly deformed material that moves in direction of metal to be cut and simultaneously roll down on the tool face. When the strain in the chips reaches a critical value, the chip fractures and the process begins over again. In this case cutting begins at a relatively high shear angle which decreases as the cutting proceeds. This type of chips are produced when the cutting speed is low or cutting material contains points of stress concentration (cast iron) or when high friction exists between tool and chips.



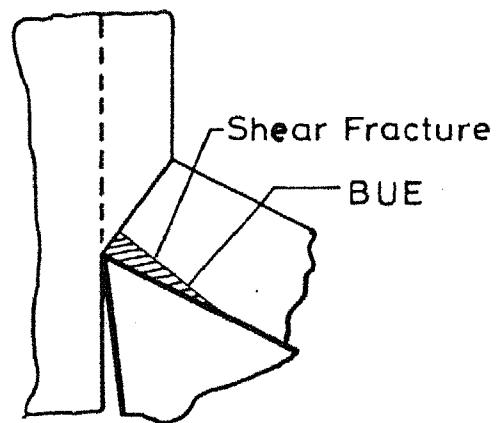
(a) Discontinuous chip



(b) Continuous chip



(c) Serrated chip



(d) Continuous chip with BUE

**Fig.1.7 Formation of different types of chips .**



(b) Continuous Chips (Without Built Up Edge)(i) Homogeneous Deformation (Regular Shape)

In crystalline ductile materials each successive element of the material passes through a narrow region called shear zone, where sliding on crystallographic slip plane occurs until it is halted by work hardening process. This shear movement is then transferred to the next lamella passing through the shear zone, thus yielding in succession and producing continuous chips Fig. 1.7(b). After the severe plastic deformation in primary shear zone it flows over the rake surface of the tool and strong adhesion between the tool and newly formed chips results in some sticking. Thus the chip material at this surface undergoes a further plastic deformation, since despite the sticking it flows. This zone is referred as secondary shear zone. Efficiency of continuous chip formation can be judged by the magnitude of the shear plane inclination.

(ii) Inhomogeneous Strain (Irregular Shape)

A continuous chip with characteristic irregular shape is shown in Fig. 1.7(c). Here shear begins at the point of stress concentration. The shear work does not have time to escape and raises the temperature on the shear plane leading to thermal softening. This causes more strain to occur on initial plane than would ordinarily occur. The shear plane then jumps to the next point of stress concentration leaving the material between relatively unstrained. Cutting with adiabatic shear

occurs with a material that has poor thermal properties (low specific heat and thermal conductivity), reasonably high specific energy, and tendency to soften at elevated temperature. Titanium and its alloys result in chip shapes of this nature.

### (iii) Continuous Chips with Built Up Edge

At the speed where the temperature at the chip tool interface is relatively low, fracture may occur within the chip along a plane approximately at right angles to shear plane. This is because of high resistance between the chip and tool face, and it results in leaving behind a portion of chip attached to the tool face (Fig. 1.7(d)). This attached material then act as cutting edge and is called built up edge (BUE). A BUE tends to grow until it reaches a critical size then passes off with the chip.

## 1.4 Previous Research

### 1.4.1 Cutting at Low Temperature

Few research workers have attempted to improve the cooling capacity of air by refrigerating it [6] Olson (1948) using cooled air in a milling operation, reported 400 percent increase in tool life over air at room temperature. Pahlitzsch has presented test results by using carbon dioxide gas and nitrogen gas as a cutting fluids. He found an improvement in tool life by about 150% using  $\text{Co}_2$  and 240% using  $\text{N}_2$  as compared to normal dry cutting.

Cryogenic cooling was first investigated around 1955 by Bortley who used liquid  $\text{CO}_2$  as the coolants. In a representative series of experiments by Leith and Heine [7] H-11, A-286, L-605, Mo - .05 Ti and R-235 (all high strength temperature resistance materials) were turned, milled, drilled and tapped in order to determine the effects of three different cooling techniques on the machining of these materials.

Cooling was accomplished by (i) application of  $\text{CO}_2$  mist at cutting edge; or (ii) floating both workpiece and tool with ABCO 156-A solvent,; or (iii) cooling the workpiece in cold chest prior to machining. Neither the mechanical properties nor the microstructure of the metals tested were significantly affected. Leeth et al. concluded that under their test condition, despite increase in tool life and cutting speed, saving could not necessarily result because of the cost of coolant, added equipment and increased machine maintenance. Cost saving resulted only from subzero machining of A-286 (solution treated and annealed high strength steel) from bar stock into the form of a unthreaded bolt, application of subzero coolants did not lessen the work hardening characteristics of this alloy.

Hellis 8 reported that during the high speed turning of various Titanium alloys, the life of carbide tool could be enhanced substantially by cryogenic cooling them with liquid  $\text{CO}_2$  around  $-78^\circ\text{C}$ . Titanium alloys are difficult to machine because of excessive work hardening, weld unbrittlement, galling tendency and higher friction. These factors result in higher cutting

point temperature and faster tool wear. Significantly improved results were obtained when the direct exposure of the interacting surface of the cutting tool to the gaseous  $\text{CO}_2$  was minimized by diverting the out flow of  $\text{CO}_2$  in a direction away from the tool and by using the neutral medium argon gas.

Feron 12 was sprayed into the clearance space between the work and tool and dramatic increment in tool life and reduction in cutting time/ $\text{mm}^3$  was observed [9]. Metals or alloys<sup>were</sup> machined with greater ease while using subzero coolant [10]. A study was made on surface finish and hardening of work materials made of stainless steel and titanium alloys at low temperature while cutting with cemented carbide tool [11]. It was established that the surface finish increases as temperature decreases.

Uhera and Kumaga [12,13] have hinted about the reduction of cutting forces and improvement in tool life and surface condition by use of liquid nitrogen. Similar observations have also been proposed by Fillippi and Ippolito [14] who conducted cryogenic face milling. Chattopadhyay et al. [15] carried out high speed turning of mild steel using a liquid Nitrogen jet as a coolant and reported that cutting forces were reduced coupled with an improvement in surface finish. Yamaya et al. [16] observed an improvement in tool life while machining with alumina ceramics tool at higher speed at cryogenic temperature.

Chattopadhyay et al. [ 17 ] have studied the relative performance of surface grinding of some common steels of varying hardness at different depth of cut by cryogenic cooling in the form of jet of liquid nitrogen. The surface after grinding under various condition were studied directly in transverse section in scanning electron microscope. They reported that use of liquid nitrogen produces the surface which are smoother and free from other damages. Benefit of cryogenic grinding for the steel considered tends to become greater with increase of grinding depth  $t$ , atleast within the range studied. Due to reduction in temperature and forces the life of wheel and dimensional accuracy is improved. Chattopadhyay et al. [18] observed that the actual temperature at grinding point came down drastically due to cryogenic cooling, the fall being about 25 to 50% of the temperature in dry grinding. Amount of temperature reduction in cryogenic grinding has been found to be reduced with increase in grinding depth  $t$  and ductility of work material. Flow zone structure of 4% carbon steel chips produced by turning at  $-196^{\circ}\text{C}$  has been studied by combination of microhardness measurement and optical scanning and transmission electron microscopy [19 ]. It was reported that pearlite change to austenite during cutting despite high heating rate ( $6 \times 10^5 ^{\circ}\text{C}/\text{sec}$ ) and short time (1.5 - 5.5 ms).

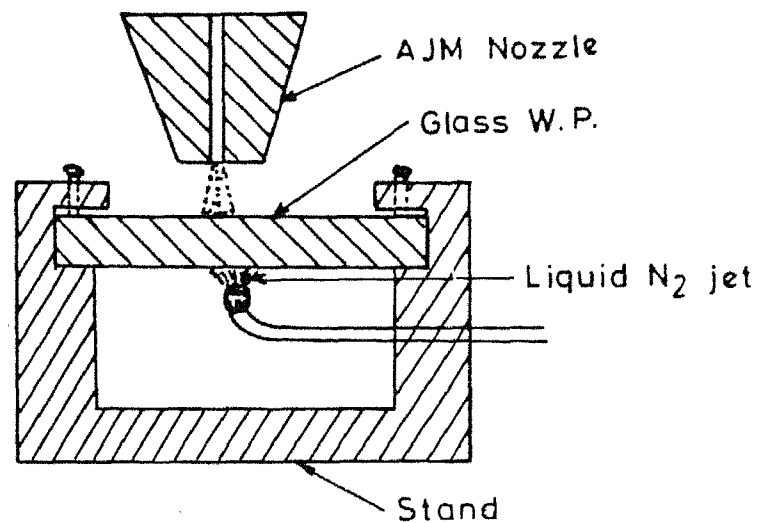
Pathak [20] has studied the effect of low temperature on the cutting forces, temperature rise, and growth in tool wear while cutting mild steel with HSS tools. Liquid nitrogen jet was used for the cooling purpose. These results showed that the cutting forces, tool wear and mean chip-tool interface temperature decreased. Shear plane angle was calculated to be increased and soft straight and bright chips were produced. In the second part of work effect of low temperature on abrasive jet machining (AJM) of glass was studied (Fig. 1.8). Experiment was carried out in abrasive jet machining unit fabricated at IIT Kanpur. These limited experiments showed that penetration and material removal increases at low temperature.

#### 1.4.2 Machining Titanium Alloys and Formation of Serrated Chips

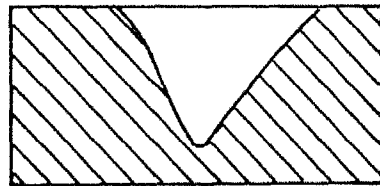
Titanium alloys are important materials for aerospace structural engineering application. They are however extremely difficult to machine, except at low speed owing to rapid tool wear [21].

Pioneering studies on machining and mechanics of chip <sup>formation</sup> alloys have been conducted since the early 1950 in the USA by Shaw and coworkers [6], Boston and coworker and Merchant and coworkers and in France by Lee Maitre and Gobin [22]. These studies illustrated several unique features with the machining of these alloys including the following:

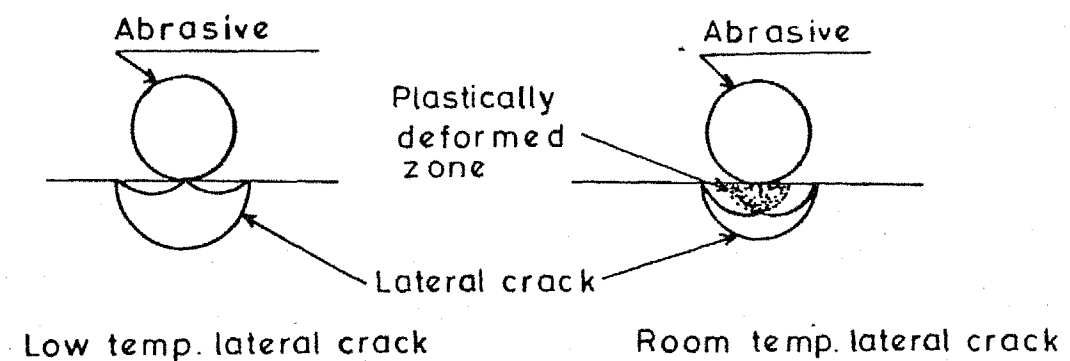
- (1) The role of the poor thermal properties of titanium alloys which interact with the physical properties in controlling the nature of plastic deformation (i.e. strain localization) in



(a) Scheme of low temperature AJM process.



(b) A typical machined cavity profile.



(c) Probable schematic diagram of lateral crack.

Fig.1.8 AJM of glass at low temperature.

the primary zone is illustrated.

(2) Periodic gross inhomogeneous deformation occurs in the primary zone (i.e. relatively low deformation forming the bulk of the segment separated by intense strain localization).

(3) Instability in the chip formation process results in a serrated or cyclic chip.

(4) Oscillations in the cutting and thrust components of force cause chatter and the need to have a rigid tool - work - machine tool system.

(5) High tool-chip interface temperatures and high chemical reactivity of titanium in machining with almost any tool material are responsible for the rapid tool wear.

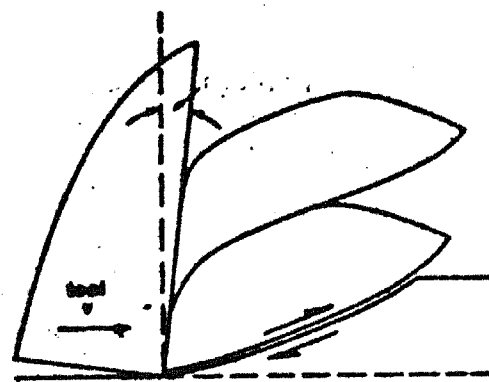
(6) The low modulus of elasticity which decreases rapidly, even at a moderate temperature (it has about 50% of its room temperature value at 400°F , causes undue deflections of the work-piece, especially when machining slender parts, and inaccuracies in the finished part.

Shaw et al. [6] suggested that chip serration of titanium alloys is due to the onset of instability in the cutting process which results from the competing thermal softening and strain-hardening mechanisms in primary shear zone. Shaw [6] also suggested that the formation of concentrated shear (adiabatic shear) was due to poor thermal properties of these alloys and consequent concentration of thermal energy in these bands.

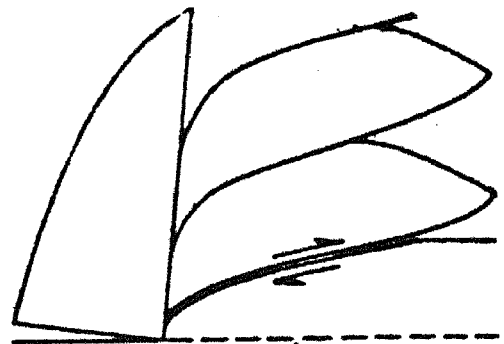


Early works by Recht [23] suggested that chip would shear locally if the rate of decrease in strength resulting from local rise in temperature equals or exceeds rate of increase in strength due to effects of work hardening. The phase catastrophic slip or adiabatic shear was used to describe the localized zones of shear and it was stated that some materials are much more sensitive to adiabatic shear than others. Nakayama [24] has attempted to explain the reason for the chip serration. He has shown cracks to form along shear plane at the free surface of the chip/workpiece boundary. It was proposed that these cracks prevented further crack initiation in the work material ahead of the tool and so determined the pitch of chip serrations.

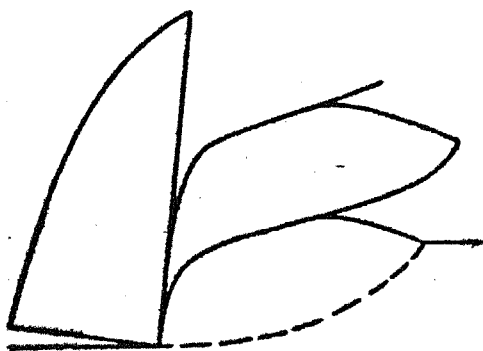
A detailed description of steps involved in the formation of one adiabatic chip has been produced [25] from machining experiments carried out inside a scanning electronic microscope. Authors reported <sup>that</sup> / there are two stages involves in this process. One stage involves plastic instability and strain localization in a narrow band in primary shear zone, leading to catastrophic shear failure along a shear surface (Fig. 1.9). The surface originates from the tool tip almost parallel to the cutting velocity vector and gradually curves in concave upwards until it meet the free surface. The other stage involves the gradual built up of the segment with low deformation by the flattening of the wedge shaped work material ahead of



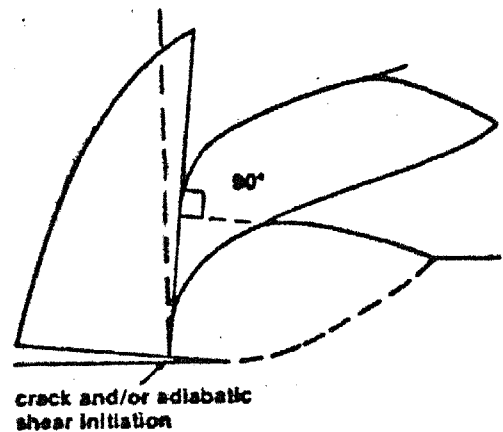
(a)



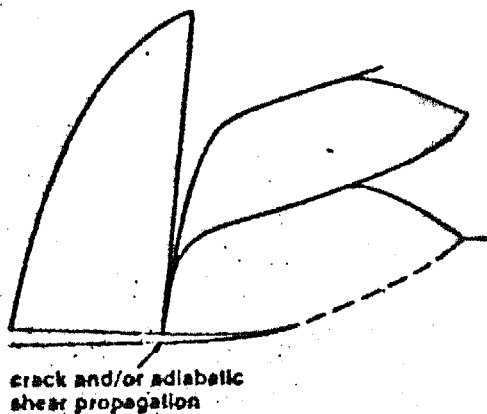
(b)



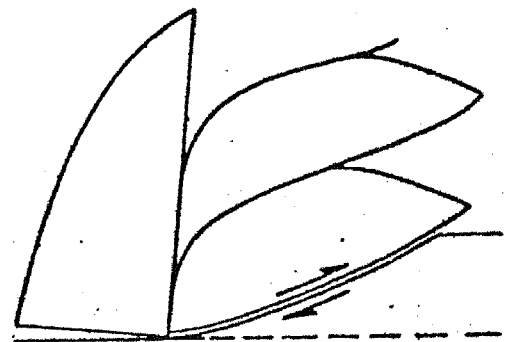
(c)



(d)



(e)



(f)

Fig. 1.9 : Schematic diagrams of a sequence of events, showing various stages involved in chip formation when machining Titanium alloys.

advancing tool. The net result is that the chip thickness will be about the same as depth of cut for orthogonal cutting and, they said that this observation led some researchers to believe, falsely, that, the shear angle is very high (about  $45^\circ$ ). They suggested that the use of term "shear angle" should be discontinued for the chip formation of this types. In their concluding remarks they reported the circumstances leading to tool wear when machining titanium alloys as (a) rolling of virgin shear failed surface of the chip on to the tool face, thereby establishing intimate contact between the tool and freshly sheared titanium during upsetting of segment under formation, (b) High temperature generation in the very narrow shear band due to extensive shear concentration in this region and poor heat dissipation from this band due to poor thermal properties, (c) high reactivity of titanium with most tool materials and (d) rapid flank wear due to the flow of material towards the clearance face like drawing operation during the upsetting stage of the chip segmentation.

As an alternative to Komanduri's description of evenys Van Luttervelt [26] has suggested a model which uses four active shear zones operating to produce one serration in a chip. The main difference between Komanduri and Van Luttervelt's model is the concept of dead-zone of built up material on the tool face. Komanduri has observed this dead zone of material in tests but has put rather more emphasis upon the effect of hot shear zone material on the tool rake face.

Based on Komanduri's sequence of events together with the inclusion of dead zone of metal Brown and Hinds [27] have described a model of the serrated titanium chips. They also obtained the variation in forces and <sup>temperature</sup> through the formation of one segment in a serrated chip (Fig.1.10).

Komanduri [22] has tried to formulate the partition of energy in the machining of titanium alloys. Figure 1.11 shows the partition of energy in detail. Owing to rapid flank wear and almost no secondary deformation on the rake face significance of zone 2 and 3 when machining titanium alloys is virtually to that for material yielding continuous chip formation. Significant portion of heat is generated at the clearance face and insignificant portion of heat is generated between the sliding chip and rake face (due to secondary shear). Also the fraction of heat carried away by the chip and getting into the tool would be different. The proposed energy partition is as follows:

$$U_c = R_1 U_s$$

$$U_t = (1 - R_1) U_s + R_3 U_{ff}$$

$$U_w = (1 - R_3) U_{ff}$$

where

$$U_c = \text{heat carried by chip}$$

$$U_t = \text{heat carried by tool}$$

$$U_w = \text{heat carried by work material}$$

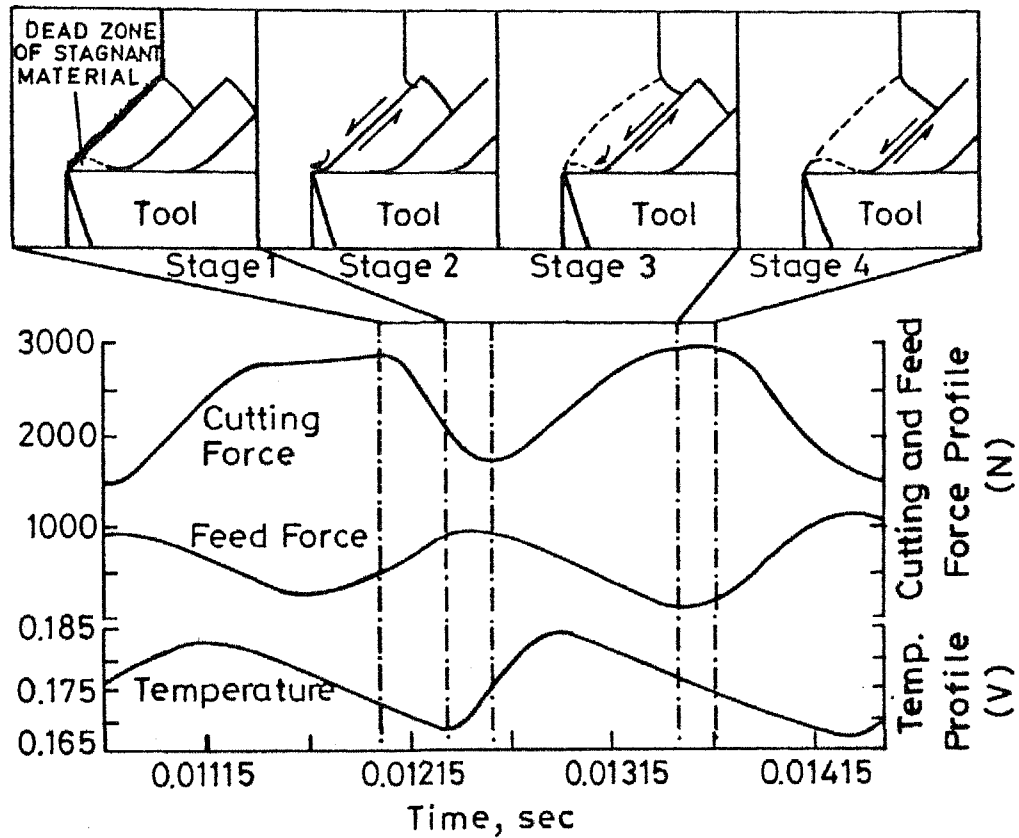


Fig.1.10 Sequence of events during the formation of one chip segment presented together with complementary force and temp. profiles.

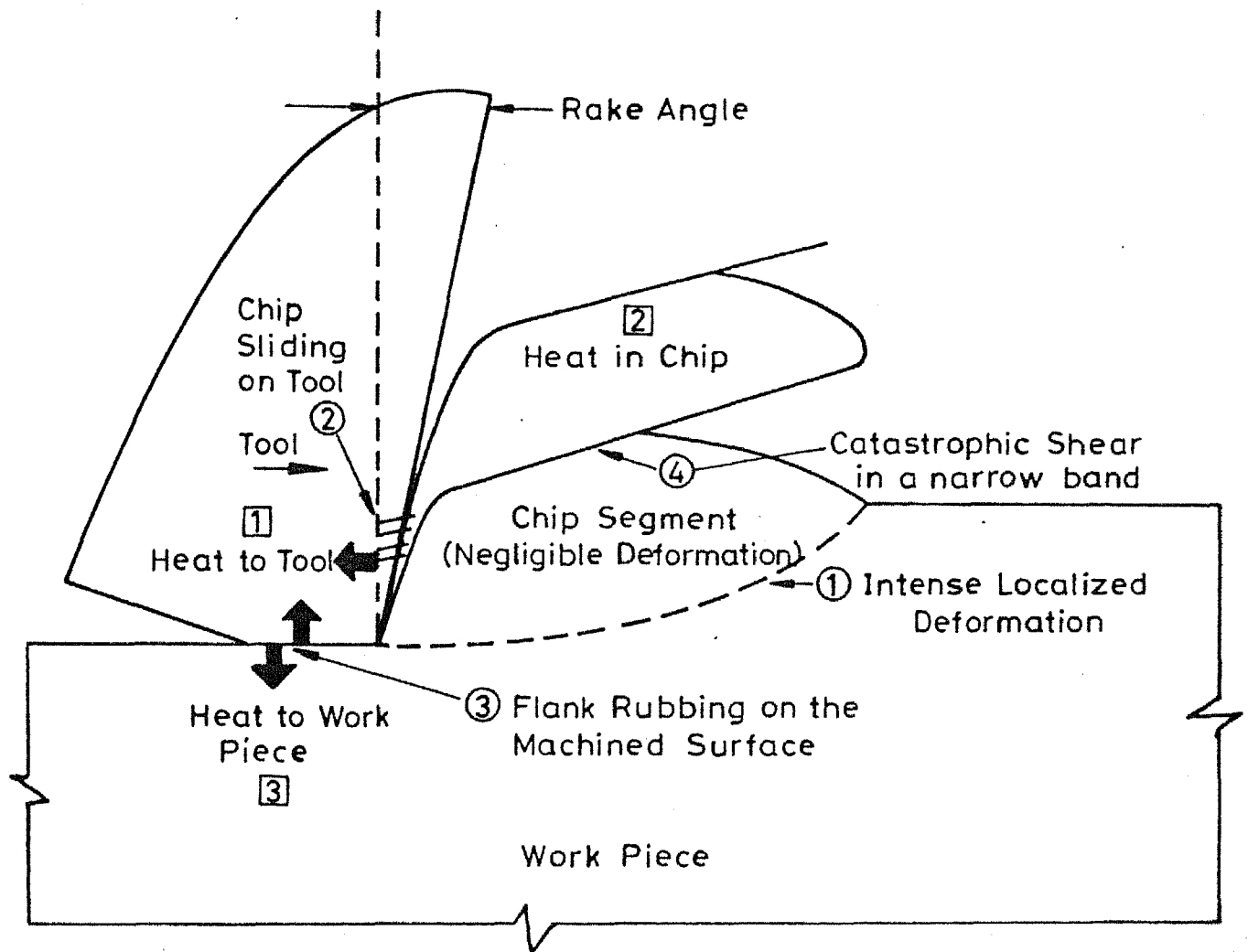


Fig.1.11 Energy partition in the machining of Ti alloys.<sup>[22]</sup>

- $R_1$  - fraction of heat going to chip from shear zone
- $R_2$  - fraction of heat going to chip from chip tool interface
- $R_3$  - fraction of heat going to tool due to flank friction.
- $U_{ff}$  - frictional energy per unit volume due to rubbing between flank and machined surface.

However, he did not explain the reason for very high temperature when cutting edge is sharp or when there is insignificant flank wear.

### 1.5 Objective and Scope of the Present Work

The discussion presented in the preceeding section clearly reveals that the machinability of various metals, alloys nonmetals, can be increased at low temperature. The basic objective of the present work was to see the what would be the effect of low temperature at in deformation zone in a machining process and the affect of variation of cooling of work material on cutting forces, keeping all other condition same. Titanium and its alloys possess low thermal conductivity high melting point, low coefficient of expansion. These unusually poor thermal properties account, to a large extent, for the difficulties in machining Titanium and its alloys. Tool wear is extremely high and the usual cutting fluids are not efficient. The original plan of the present work was therefore to investigate the machining of Titanium and its alloys at low temperature at

length to observe the wear. However due to considerable difficulties in procurement of Titanium alloys work was confined to the machining of mild steel in first phase, and in second phase to the commercially pure Titanium. For cooling liquid Nitrogen has been used to create low temperature in cutting zone or to cool work material.

The cutting forces tool-chip interface temperature and mechanism of chip formation have been investigated.



## CHAPTER 2

### MACHINING IN LIQUID NITROGEN ENVIRONMENT

#### 2.1 Introduction

If we consider the wear of the cutting tools, the effect of conventional coolants <sup>are</sup> is not always positive. Almost all the cases coolants reduce the interface temperature but do not always increase the tool life (Fig. 2.1). It has been reported that though the coolant carries some heat away from wear <sup>land</sup>, it simultaneously shifts the maximum temperature closer to the tip, which enhance further wear at tool tip. Under such circumstances cryogenic cooling by agents like liquid nitrogen may meet the challenge offered by heat and its effects.

Also the properties of materials with bcc, hcp structure change drastically at low temperature; so, instead of cooling only the cutting zone, if the work material could be cooled to cryogenic temperature, additional advantage in the form of change in properties can be achieved. Keeping this in view the machining under liquid nitrogen environment is undertaken and accordingly setup is designed.

#### 2.2 Experimental Setup

For the present work a hmt centre lathe with step variable spindle speed and feed was used. The head stock which is powered by a DC motor was incorporated with a four-jaw chuck to hold work material with accuracy.

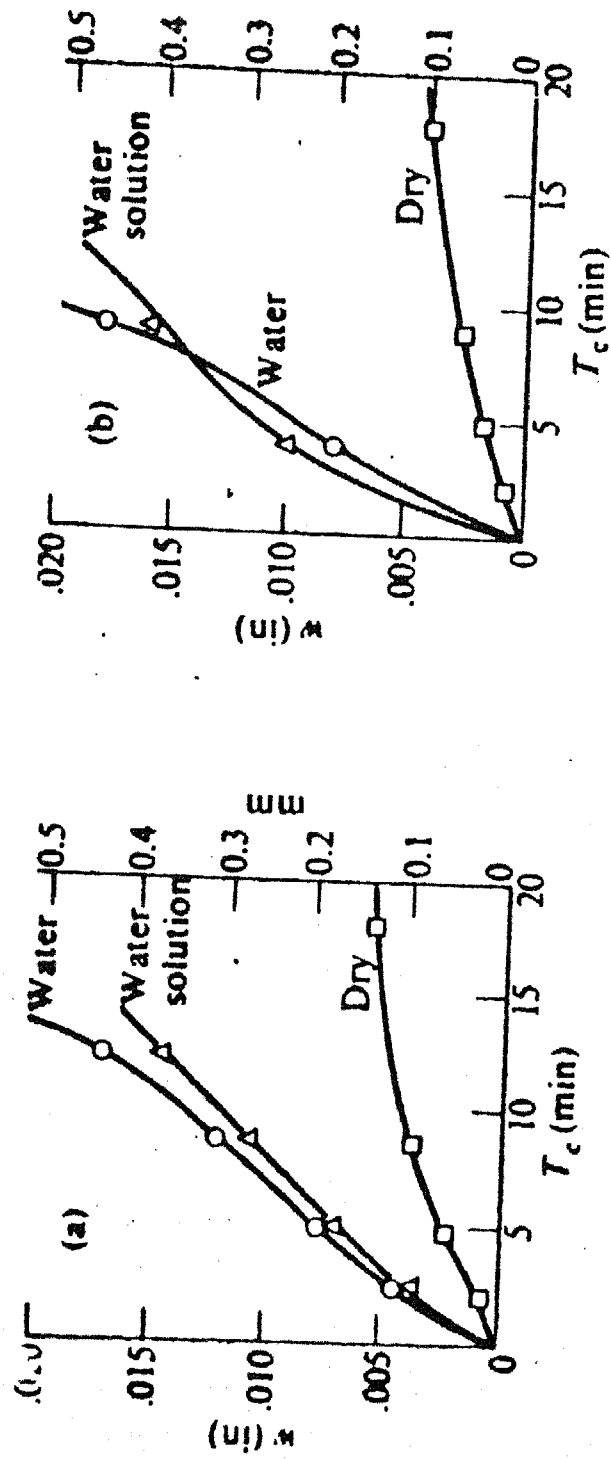


FIG. 2.1. VARIATION OF WEAR LAND ( $W$ ) WITH CUTTING TIME  $T_c$  FOR DIFFERENT CUTTING FLUIDS.  
 (a) AISI 1020 STEEL MACHINED WITH HSS TOOL.  
 (b) AISI 4340 STEEL MACHINED WITH HSS TOOL.

### 2.2.1 Experimental Setup for Cooling Arrangement

The experimental set-up is schematically shown in Fig. (2.2). For cooling one fully filled liquid nitrogen container of 26 litre was taken and was kept at the same level as of cutting point to reduce the length of tubing required for supply of liquid nitrogen. This kept the loss of heat to surrounding to a minimum.

#### Distributor

A simple four way liquid nitrogen distributor system was fabricated and welded to a copper tube - which carried liquid nitrogen from the bottom of the liquid nitrogen flask to the mouth of vessel. Distributor was made of copper to avoid corrosion and brittleness in liquid nitrogen atmosphere. While manufacturing, great care was taken to avoid any possibility of leakage. For this purpose, the number of joints were kept as low as possible. All the four cocks were welded at equal angle with each other to the top of distributor. Spring loaded valves were used in cocks to minimize leakage, flow of liquid nitrogen could easily be controlled by regulating the cock lever.

#### Nozzle-Holding-System

A nozzle handling device was designed and fabricated to hold the nozzles in position around the workpiece while performing cutting operation. Holding device was designed so that liquid-nitrogen could flow out either on the face of work material (as in the case of a pipe) or on the cylindrical surface (as in the

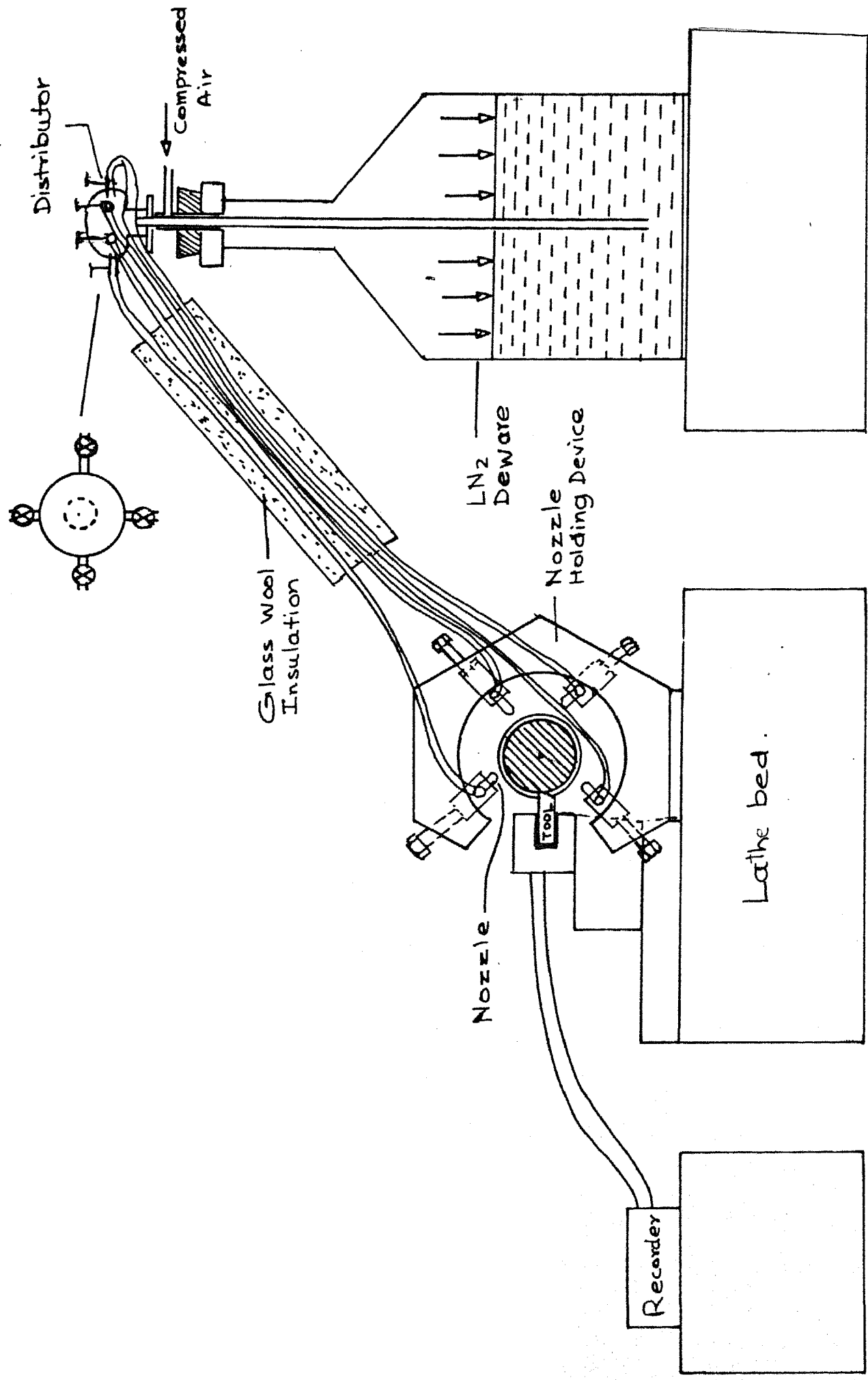


Fig.2.2 Schemetic diagram showing cooling arrangement .

case of a rod). Figure 2.3 shows the diagram of holding device. The whole system was mounted on the tool carriage so that it also moved with the tool during the operations. To adjust the gap between the work material and nozzle tip, screw were provided at the holding position of each nozzle.

### Nozzle

Four converging nozzles of aluminium were manufactured so that liquid nitrogen comes out with sufficient velocity from the nozzle irrespective of the position of nozzle around the work-piece. A diameter of the holes at input and output of the nozzle were kept 6 and 1.5 mm, respectively in the length of 55 mm. A continuous taper could not be provided due to manufacturing difficulties. Step drilling was done to get reduction in diameters. Serration at inlet was provided for leakproof fitting

### Tubing&Insulation

Four tubes of plastic ~~serration~~ were used to carry liquid nitrogen from distributor to nozzles. A very good insulation of glass wool of 60 mm thickness was provided in the middle part of tubes and insulating rubber tubes (used for refrigeration) were used as insulating material at the beginning and end of the plastic tubes. These rubber insulating tubes having inner diameter of 7 mm and thickness of 5 mm were found to be satisfactory, and minimized the possibility of breaking of the plastic carriage tubes which become brittle at low temperature and tend to break when nozzle end of the tubes move towards head-stock.

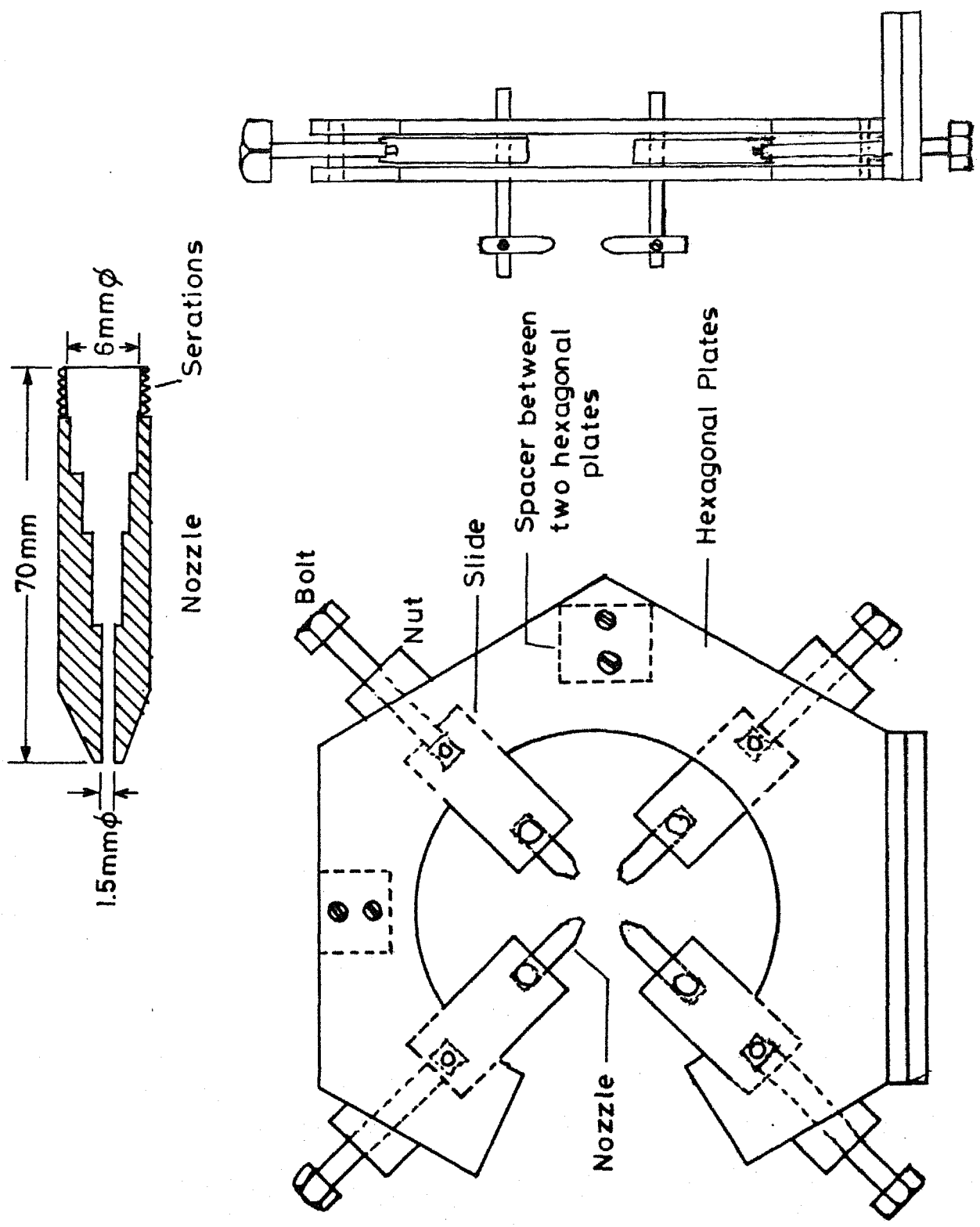


Fig. 2.3 Device for holding nozzles in position.

### 2.2.2 Experimental Set-up for Force Measurement

As the cutting was of orthogonal type, the force in the direction of tool axis was zero, so only two component of forces that is cutting force and feed force were measured using a lathe tool dynamometer. DC supply (of 7 volt. ) was used for exciting the measuring strain gauge bridges. In order to record and analyse the results, the dynamometer was connected to a recorder which gave readings in mV. Keeping all conditions same, the dynamometer was calibrated for both the forces. Increasing loads through standard weights were applied. On the basis of load and the corresponding deflection obtained by recorder, a calibration chart was made. It is shown in Fig.2.4. It can be seen from the calibration curves, that it is linear upto the applied load. This curve can be extrapolated for higher values of load.

### 2.2.3 Set-up for Temperature Measurement

The most extensively used method for tool chip interface temperature measurement, uses the tool and work material as the two elements of a thermocouple. The laws of thermoelectric circuit that are applicable here are summarized as follows:

- (1) The emf in thermoelectric circuit depends only on the difference in temperature between the hot and cold junctions, and is independent of the gradients in the parts making up the system.
- (2) The emf generated is independent of the size and resistance of the conductors.

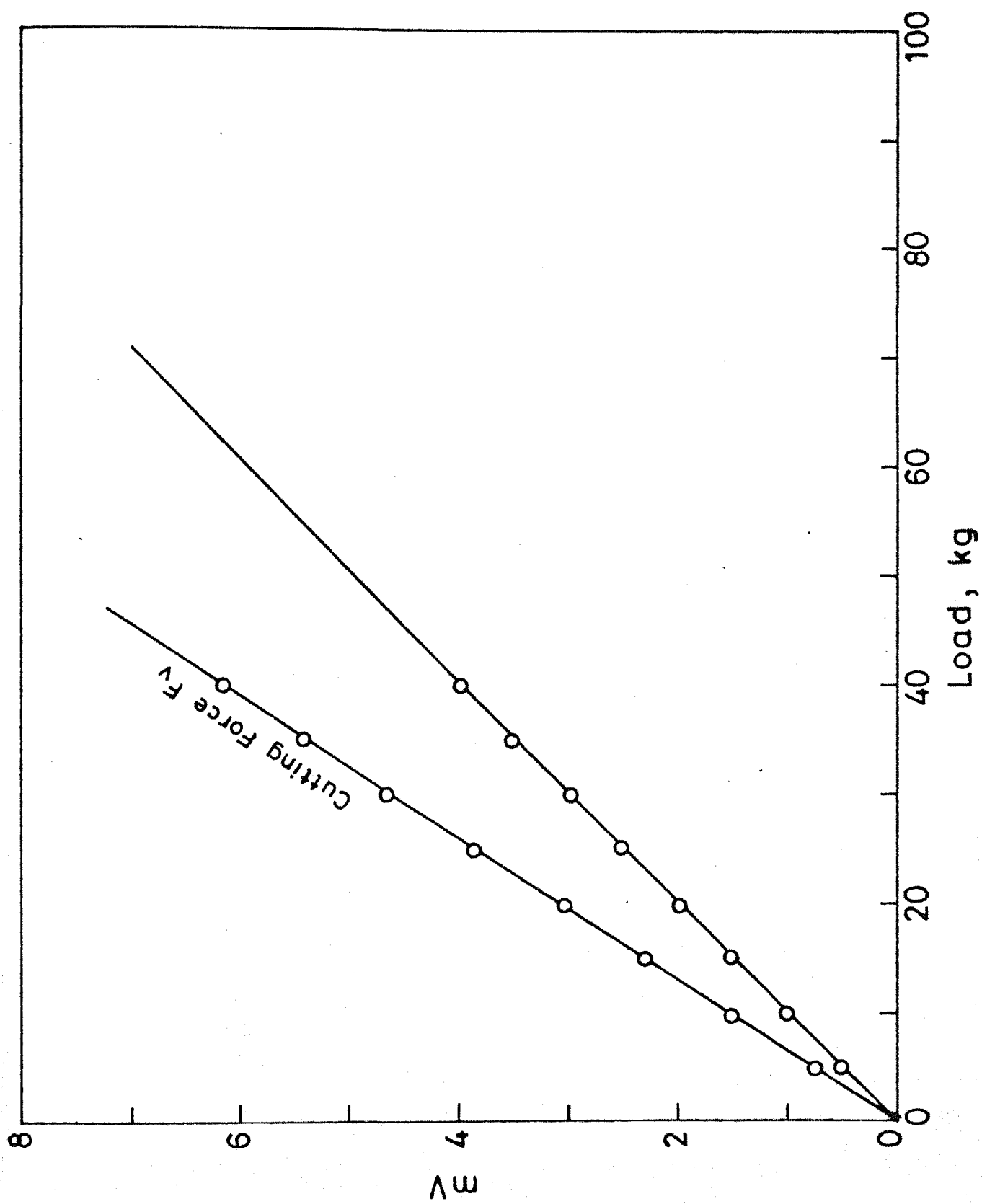


Fig. 24 Dynamometer calibration curve. Input voltage = 0.7 Volt



(3) If the junction of two metals is at uniform temperature, the emf generated is not affected if a third metal which is at the same temperature, is used to make the junction between the first two.

In the tool work thermocouple shown in Fig. 2.5, cutting tool and workpiece were electrically insulated from the lathe machine. One threaded mild steel bar was screwed to the end of the workpiece and on the other end of the bar a copper disc was mounted. To make a continuous contact the copper disc was kept in a mercury bath. Similarly a copper wire was soldered to the HSS tool to complete the connection. The chip and tool junction H constituted the hot junction, while A and B, cold junctions, remained at room temperature. An 'Omniscrite' recorder was used to record the emf generated in the operation. For proper correlation and to save cutting material and tool, it was decided to measure temperature and force at the same time. To avoid the heating of the cold junction, cutting was performed for short duration, and also while cutting steel only 10% of the total heat generated goes to tool which further reduced the possible error in measurement, and steep temperature gradient occurred. Calibration of tool work thermocouple was carried out (Fig. 2.6) A standard thermocouple of Alumel Chromel was used and was also connected to recorder. Hot junctions of both the thermocouples were dipped in a lead bath to record the same temperature. Temperature of furnace was found by the reading standard thermocouple and was related to the emf of thermocouple

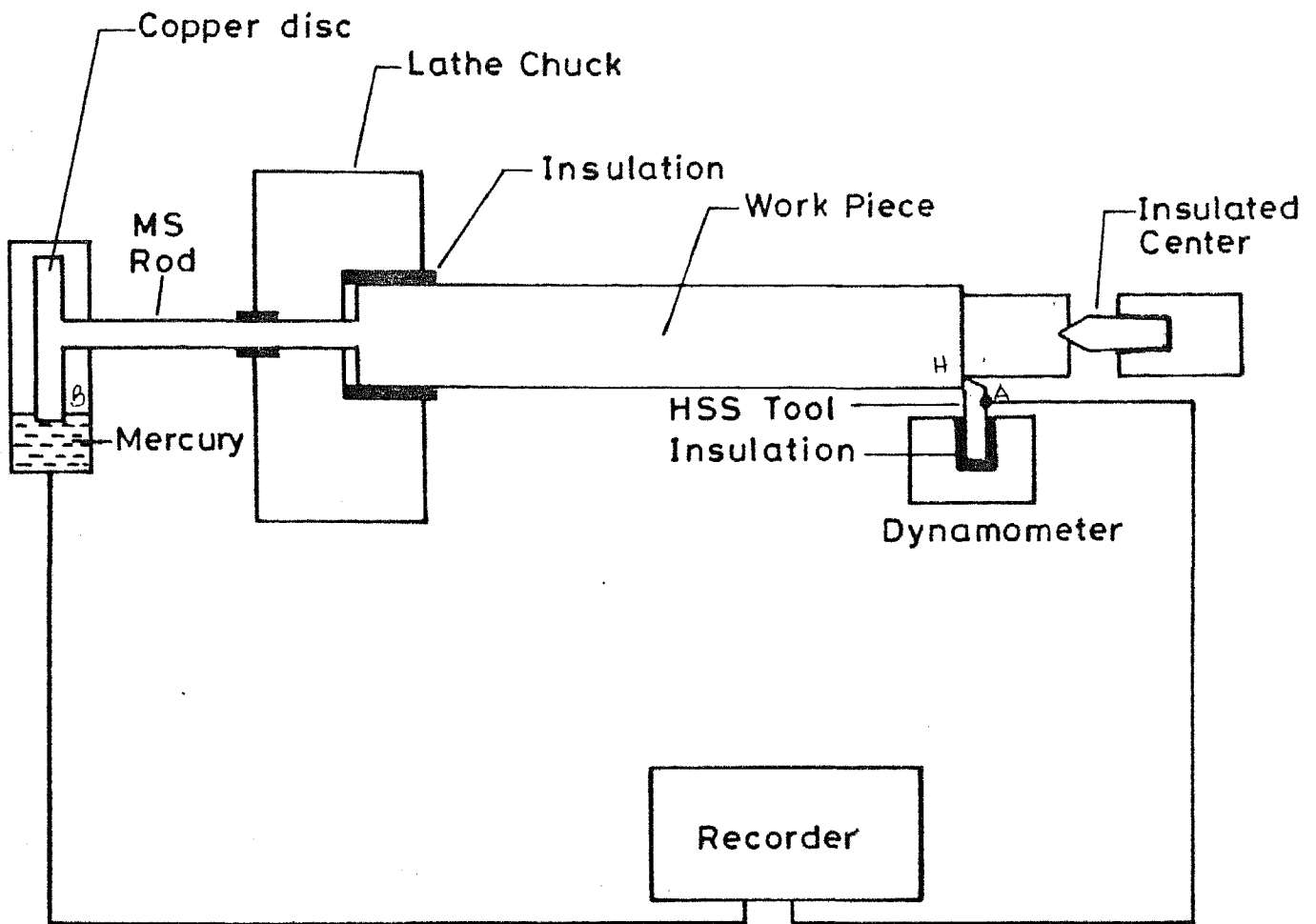


Fig. 2.5 Schematic diagram for measuring chip tool interface temperature.

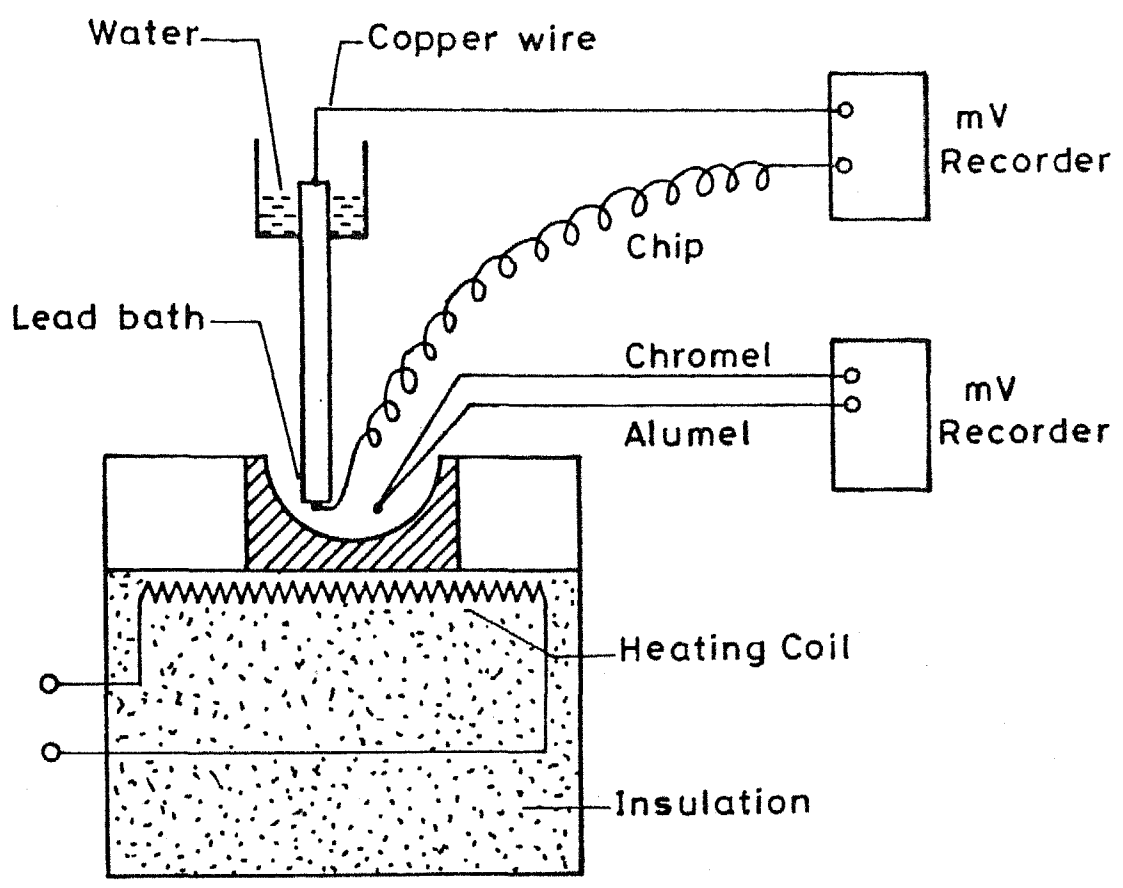


Fig. 2.6 Arrangement for calibration of tool work thermocouple .

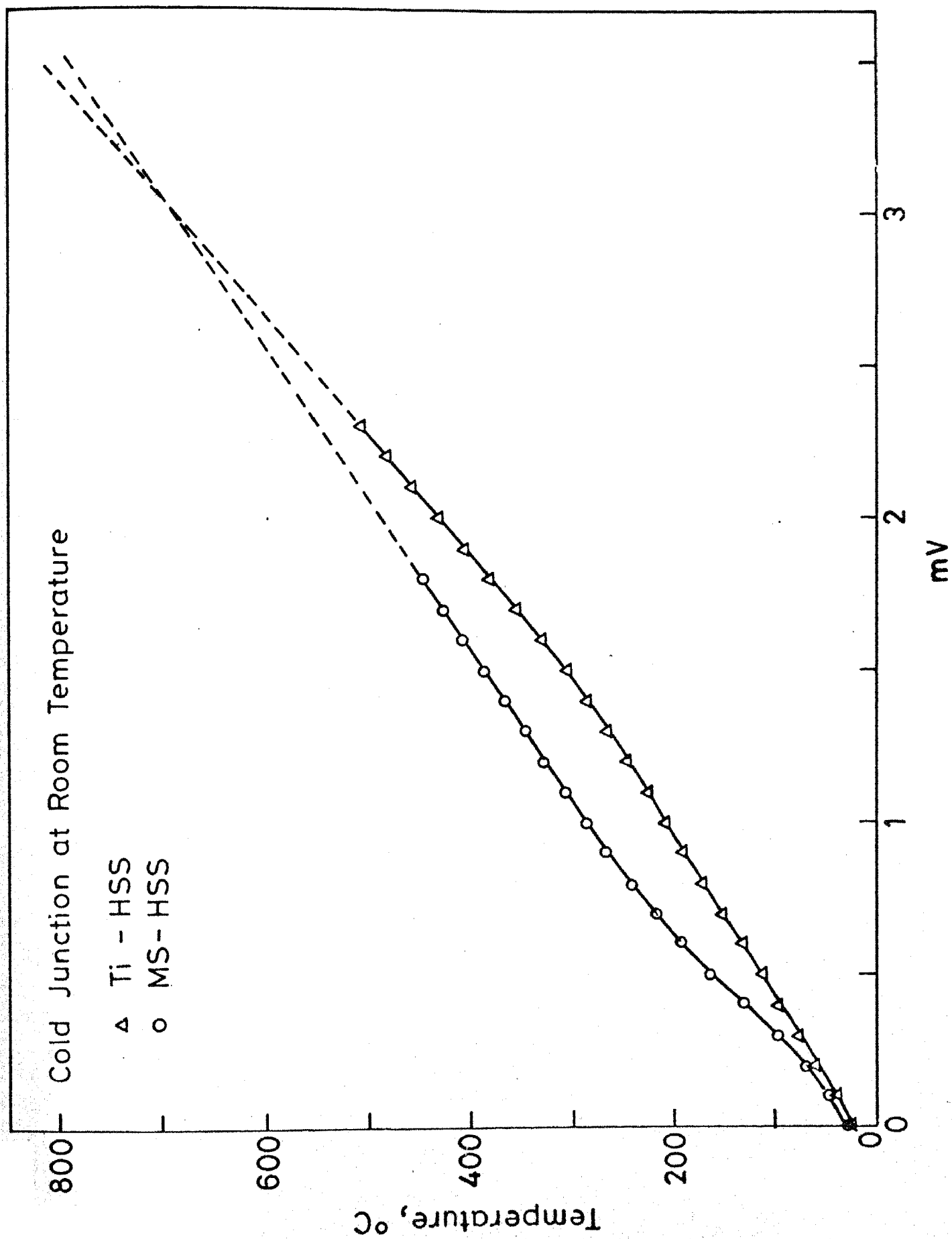


Fig 2.7 Temperature calibration curve of mild steel and titanium with HSS.

to be calibrated. Figure 2.7 shows the calibration curves for mild steel-HSS and Pure Titanium - HSS thermocouple.

## 2.3 Tool Material

In the present set-up high speed steel was used as the cutting tool material. The dimensions of each tool were taken as 55x10x10 mm, keeping the bore dimensions of the dynamometer (33x12x12 mm) in view. Cross section of the tool was taken less so that electrical insulation could be provided around the tool. Tool over hang was kept 18 mm. The tool geometry was kept as follows:

Angle	Value
Bake Rake	0°
Side Rake	12°
End clearance	6°
Side clearance	7°
End cutting edge	6°
Side cutting edge	0°
Nose radous	0

Some experiments at room temperature were also conducted with straight grade carbide inserts with an edge radius of 40  $\mu\text{m}$  to avoid buildup edge formation. Standard tool holder was used with following tool geometry.

Angle	Value
Bake Rake	- 0°
Side Rake	- 5°
End clearance	- 11°
Side clearance	- 6°
End cutting edge angle	-15°
Side cutting edge angle	-15°
Nose radius	- .8 mm

However due to difficulties in mounting on the dynamometer and large overhang, large vibration were observed even with less feed and small depth of cut, so it was not used for further experiments.

#### 2.4 Work Materials

Test were mainly conducted on mild steel bar of 96 mm diameter and phase commercially pure titanium (RT 12 - Hardened and Annealed) of 48 mm diameter. The following table gives the properties of the material used:

Tensile Properties	Commercial Pure Titanium	Medium Carbon Steel
Elastic modulus $\times 10^6$ Psi	17	30
Yield strength (2% Ksi)	86	49
Ultimate strength (Ksi)	100	86
Elongation (%)	50	25
Reduction of Area %	35	60
Thermal conductivity cal/cm <sup>2</sup> -cm-°C	.05	.18
Density	4.5	7.8
Vol. specific heat (cal/cm <sup>3</sup> -°C)	.56	.86
Thermal expansion (micro inch/in °C)	8.4	11.3
Approximate ductile brittle transition	-160°C	RT

## 2.5 Experimental Procedure

### Dry Cutting

Mild steel bar insulated from machine was held in headstock and a HSS tool with proper insulation was fastened to the dynamometer, as mentioned earlier. Work material was made insulated from tailstock by providing a thin sheet of insulating material (Fig. 2.5) on the taper side of centre. A feed of .05 mm/rev was selected and constant depth of cut of 2 mm was used throughout. Cutting operation was first performed at low rpm. Dynamometer connected to the double channel 'Omniscribe' recorder, directly

88342

recorded the two components of forces on graph paper. Similarly, the tool-chip interface temperature was recorded by other recorder. Cutting operation was continued till recorder system indicated stable deflection. <sup>After completing experiments with one open</sup> At this stage the tool post was taken back and other tool with sharp edge was fastened, and the same operation was repeated for higher rpm. After doing one set of experiments, another set was performed by changing the feed to .125 mm/rev. For each feed the experiments were performed at really different speeds.

#### With Liquid Nitrogen

Experiments were performed by varying 'the number of nozzles open' during turning. Air under a pressure of  $2\text{kg/cm}^2$  was sent on the top surface of liquid nitrogen, which compressed the liquid to flow out through central copper pipe in the form of a jet. Only one cock of the four way distribution system was kept open and the liquid nitrogen jet was applied on the surface of rod through the nozzles as per plan. Only after sufficient precooling had occurred the experiment was performed. After doing one set of experiments, the other sets were performed by opening, two nozzles and four nozzles, respectively. For each cutting operation a fresh tool was used. Tests were conducted at feed rates of .05 mm/rev <sup>and</sup> .125 mm/rev

At .125 mm/rev feed one extra set of experiment was conducted by applying the jet of nitrogen on the work material ahead of cutting zone as shown in figure.



Commercially <sup>pure</sup> the titanium was also machined with and without liquid nitrogen. Experimental procedures were same except for the depth of cut which was taken as 1mm in the latter case. In the beginning, experiments were conducted with 2 mm depth of cut but due to large chattering and galling problem, it was decided to conduct experiments at lower depth of cut of 1 mm. When cutting Ti with liquid nitrogen, experiments were conducted using four nozzles only, for both feeds (0.5 m/rev. and .125 m/rev.). It became <sup>necessary</sup> because of the problem in procurement of liquid nitrogen.

## CHAPTER 3

### RESULTS AND DISCUSSION

#### 3.1 Machining of Mild Steel

The various experimentally obtained and calculated results for machining of mild steel are tabulated in Tables 3.1 to Table 3.9 and are plotted in Figs. 3.1 to 3.11.

##### 3.1.1 Cutting Temperature

Figure 3.1 and Figure 3.2 shows how the temperature is reducing for different feed when liquid nitrogen is used for cooling purpose. It can be seen from Fig. 3.3 that as the rate of flow of liquid nitrogen (number of nozzle) on the work surface is increased the percentage reduction in chip-tool interface temperature also increases. But the increase is showing a kind of a saturation at high rate of flow. This can be explained apparently as below.

The fraction of heat generated at shear plane going to workpiece remains independent of quantity of  $LN_2$  flow then the chip tool interface temperature should also rise in the same proportion as the increase in heat flow into the chip.

Apparently upto some flow rate there is increase in heat withdrawal from shear zone, causing the interface temperature to fall sharply. Beyond a certain heat withdrawal rate (in the region of two nozzles (Figure 3.3) interface temperature does not fall so sharply.

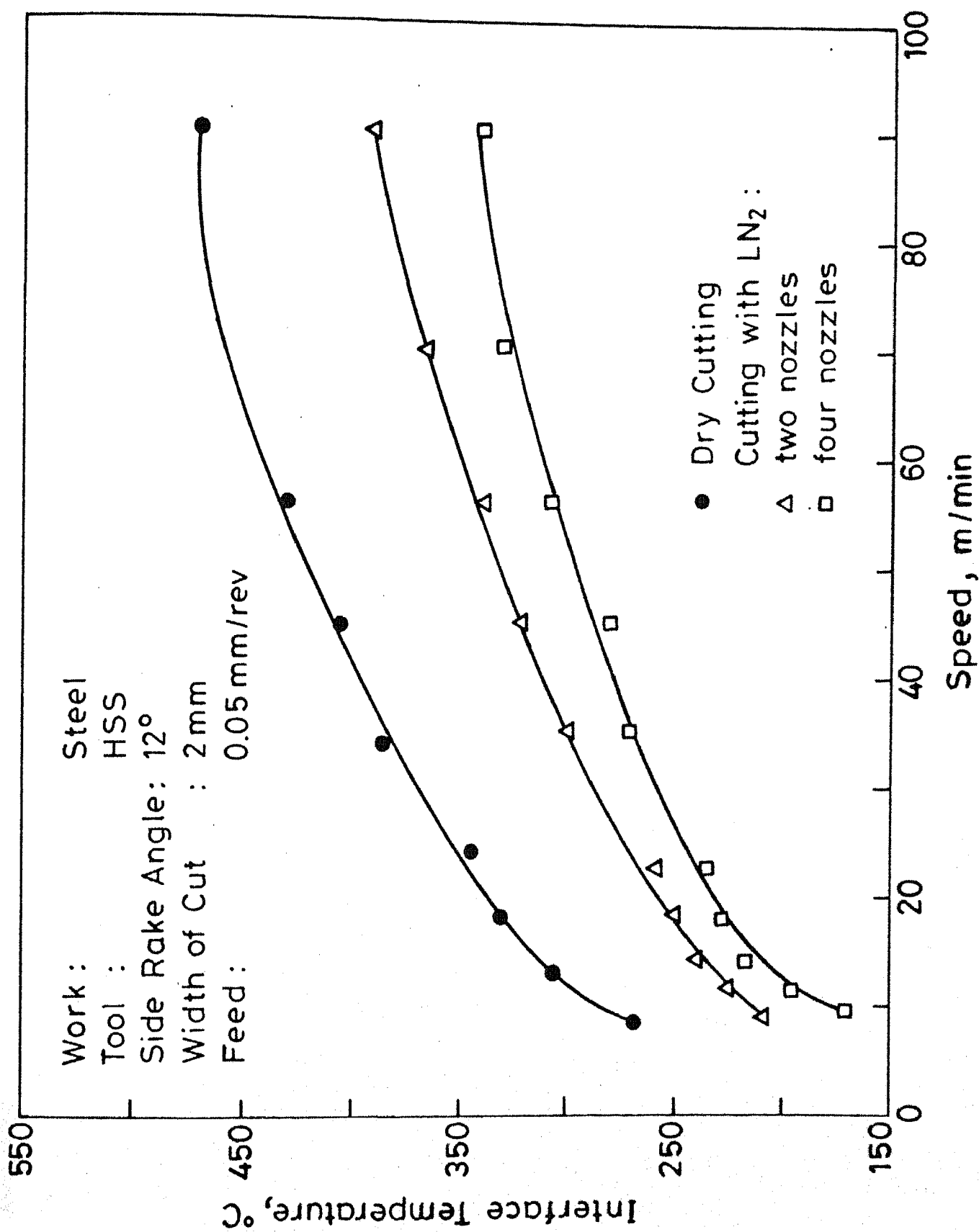


Fig.3.1 Variation of interface temperature with speed (experimental)

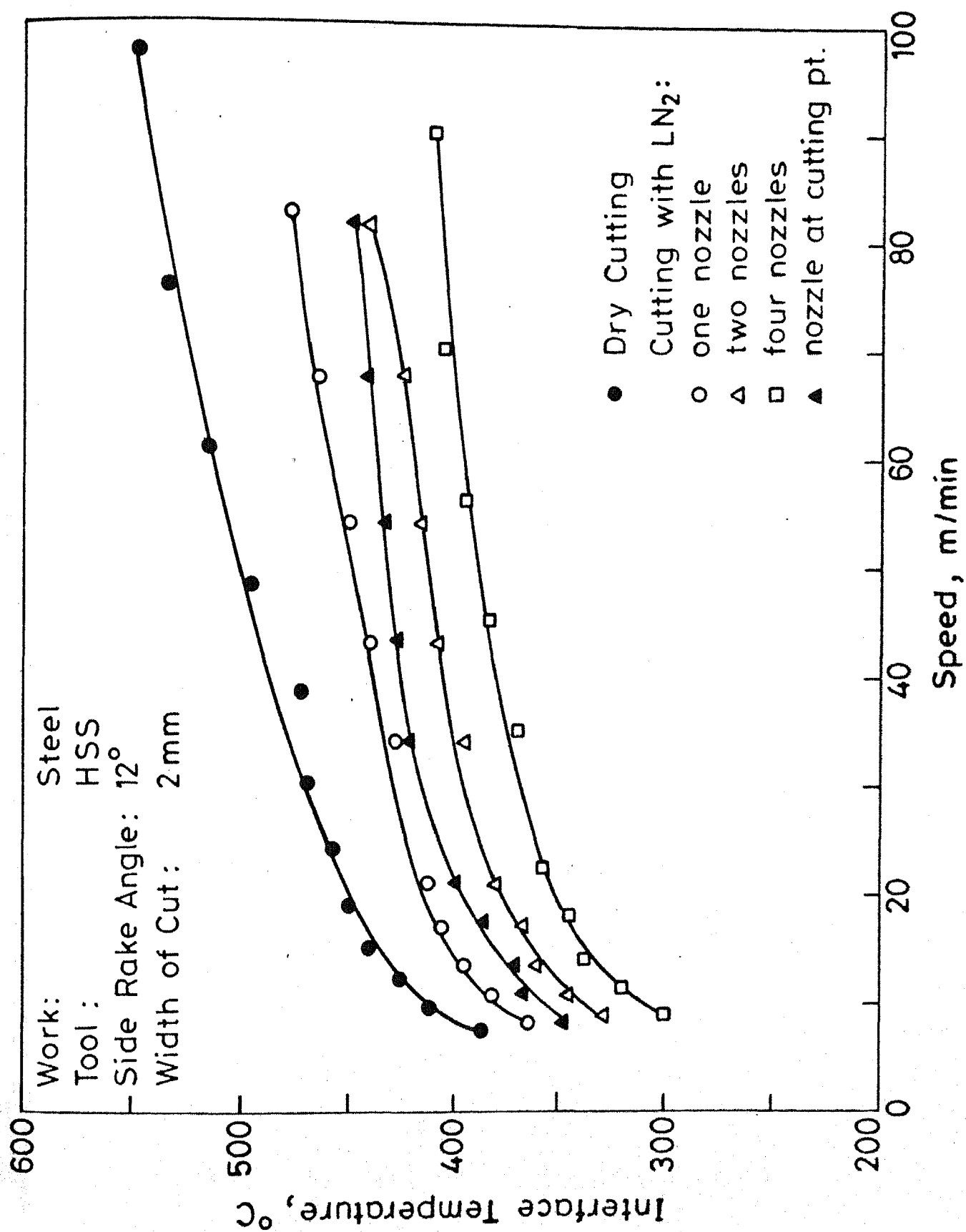


Fig.3.2 Variation of interface temperature with speed (experimental)

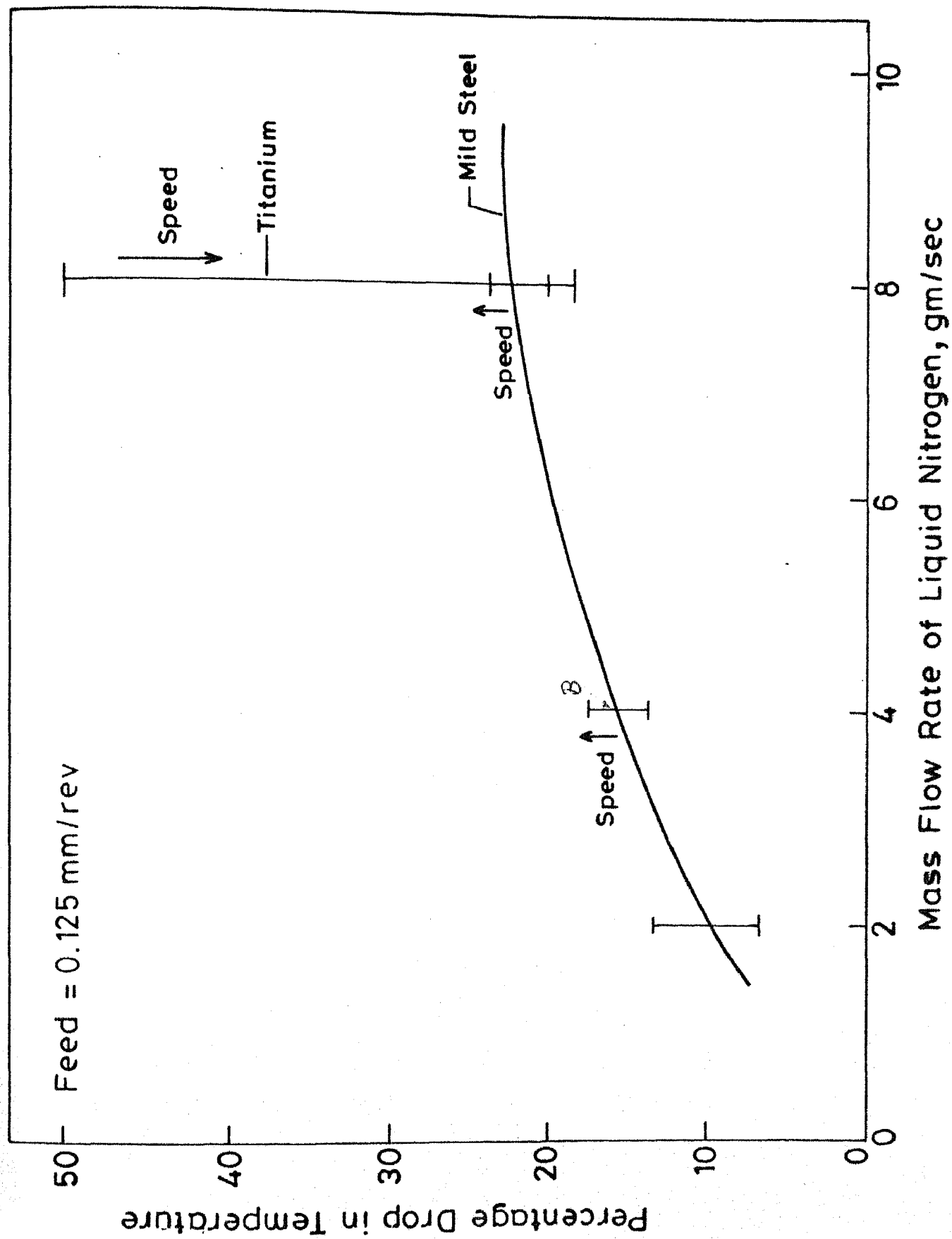


Fig. 3.3 Range of percentage fall in temp. with mass flow rate of liquid nitrogen

It can also be seen that fall of temperature is more at higher speed but overall percentage fall is decreased with speed (Fig. 3.4). With increase in feed, percentage reduction in chip tool interface temperature also decreases.

### 3.1.2 Cutting Forces

Figures 3.5 and 3.6 (and Table 3.1 and 3.2) show the variation of cutting force  $F_c$  with velocity for different cutting environment. Variation of feed force  $F_t$  is tabulated in Tables 3.1 and 3.2 for two different feeds. From the experimental results it is clear that cutting forces are showing slight decreasing trend with increase in velocity. Actually the cutting force gets affected by shear plane angle. As shear plane angle increases, shear plane area decreases, hence tool undergoes less plastic deformation. Cutting force also depends upon the tool-chip contact length and nature of chip. It can be seen that cutting force ( $F_c$ ) was decreased significantly when liquid nitrogen was used. Drop in the above-mentioned forces increases with increase in mass flow rate of liquid nitrogen atleast within the present range of study. However tables 3.1 and 3.2 show that change in feed force  $F_t$ , when liquid nitrogen is supplied on cylindrical surface of work is very insignificant. Probable reason for the observed nature of the feed force with use of liquid nitrogen (when cutting force is decreasing) is the increase of mean coefficient <sup>of</sup> friction between tool and chips. Variation of  $\mu$  is also shown in Fig. 3.7 for a feed rate of .05 mm/rev. In column 7 of Table 3.2 the variation of  $\mu$

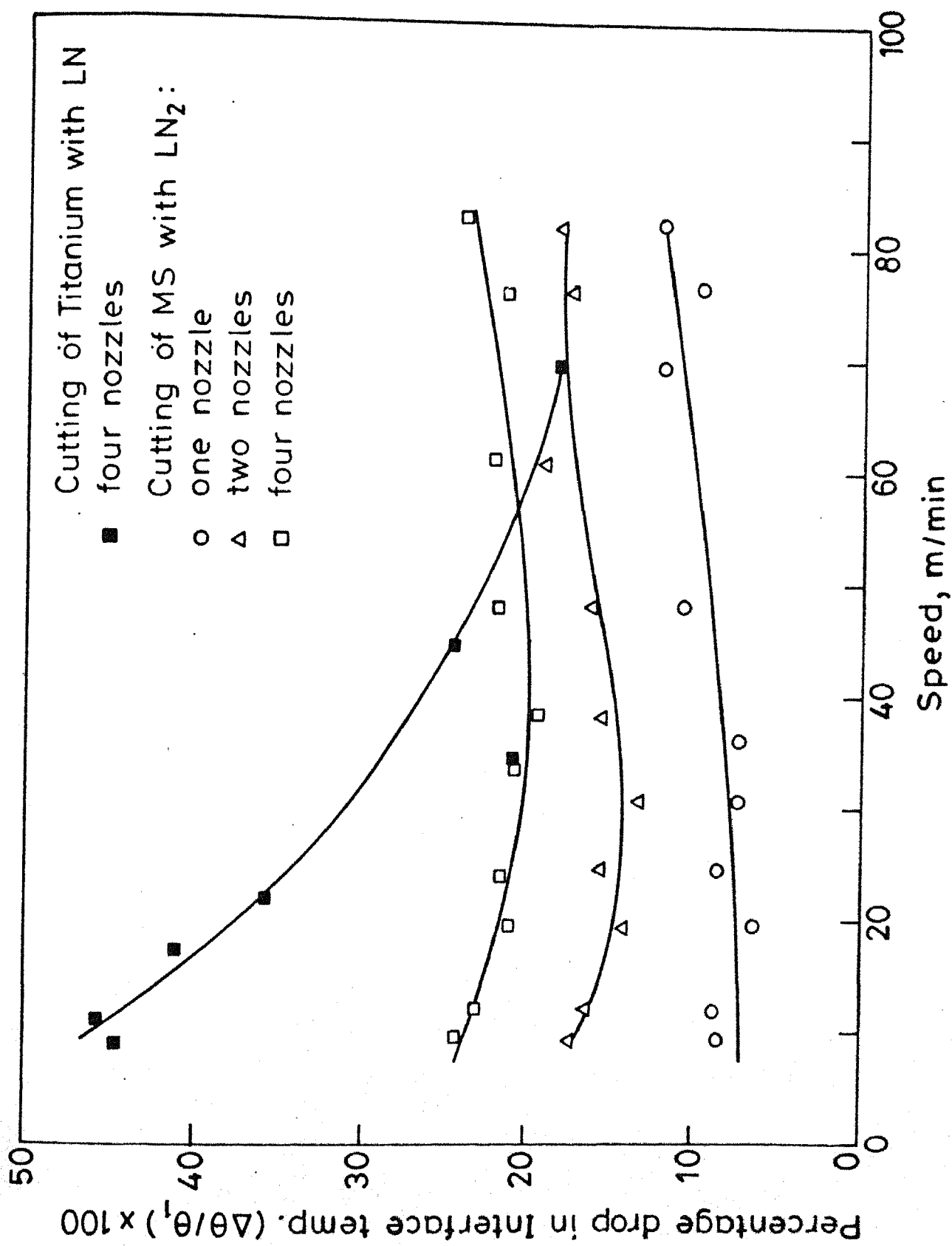


Fig.3.4 Variation of percentage drop in interface temperature with speed.  
 Feed = 0.125 mm / rev

TABLE 3.1 : Comparison of shear plane angle  $\phi$  and  $\phi_{EM}$ 

$F_c$  - cutting force, Work - Mild steel, Width of cut = 2mm  
 $F_t$  - feed force, Tool - HSS, Feed = .05 mm/rev.  
 $\phi$  - shear angle from shear plane theory, Side rake angle = 12°  
 $\phi_{EM}$  - Shear angle obtain from Ernst-Marchant Theory

Cutting condition	$V$ m/min	$F_c$ kg	$F_t$ kg	$r$	$\phi$	$\mu$	$\phi_{EM}$
Dry	8.52	31.2	20.0	.4826	27.68	0.988	28.520
	13.32	37.05	25.0	.41039	23.69	1.035	28.007
	17.47	33.80	23.0	.42400	24.462	1.04403	27.88
	24.64	30.00	20.0	.4605	26.48	1.0243	28.15
	34.10	29.25	19.0	.4600	26.42	1.00	28.50
	45.00	28.00	18.0	.5424	30.88	0.228	28.50
	56.27	28.00	20.0	.51	29.55	1.09	27.26
	90.00	29.00	20.0	.50	29.50	1.04	27.93
	9.027	27.00	23.0	.445	25.62	1.299	24.79
	14.137	28.75	24.0	.4642	26.88	1.273	25.075
LN <sub>2</sub> with two nozzles	18.095	29.37	24.5	.4653	26.74	1.273	25.025
	22.619	26.25	21.0	.55	31.20	1.272	25.080
	35.34	24.37	20.0	.474	-	1.220	25.670
	56.57	23.75	19.0	.650	36.00	1.22	25.600
	70.685	23.12	19.0	.550	312.00	1.252	25.65
	90.477	23.00	19.5	.395	22.8	1.290	24.70
	141.47	22.50	19.0	.350	20.65	1.280	24.80

Continued.....



TABLE 3.2 : Comparison of Shear Plane Angle and  $\phi$  and  $\phi_{EM}$

Work - Mild steel, Tool- HSS, Side Rake angle=12°,  $F_c$  - cutting steel,

Width of cut = 2mm, Feed = .125mm/rev,  $F_t$  - Feed Force,

$\phi$  = Shear angle from shear plane theory,  $\phi$  - Shear angle from Ernest Marchant The

Cutting condition	V m/min	$F_c$ kg	$F_t$ kg	r	$\phi$	$\mu$	$\phi_{EM}$
Dry cutting	7.71	64.5	47.5	0.55	31.00	1.125	26.81
	9.75	66.3	49.0	0.5195	29.69	1.1289	26.76
	15.54	64.35	46.0	0.577	30.00	1.439	23.39
	19.50	61.40	47.5	0.529	30.173	1.169	26.27
	38.50	61.10	48.0	0.448	25.770	1.192	25.99
	60.90	59.15	46.0	0.3631	21.000	1.103	20.08
	76.00	58.50	45.5	0.3682	21.300	1.164	26.00
LN <sub>2</sub> with one nozzle	8.64	60.00	47.0	0.545	31.01	1.148	25.20
	13.50	58.125	45.0	0.563	31.96	1.181	26.126
	17.29	58.75	46.0	0.550	312.00	1.194	25.973
	33.72	56.25	45.0	0.570	323.0	1.220	25.67
	48.22	55.625	44.5	0.51	29.26	1.22	25.67
	54.03	55.00	44.0	0.497	22.47	1.221	25.67
	67.54	54.32	44.0	0.481	22.50	1.72	2.563
	86.456	52.75	43.50	0.462	26.69	1.243	25.400
LN with two nozzles	08.64	58.125	46.00	0.529	30.20	1.206	25.82
	13.50	56.95	44.00	0.576	32.62	1.180	26.10
	17.29	57.50	46.00	0.5702	32.32	1.200	25.69
	33.72	52.00	46.00	0.573	32.46	1.300	25.38
	43.22	15.00	45.00	0.5310	30.32	1.500	25.36
	54.63	52.75	44.00	0.492	28.19	1.230	25.54
	47.54	52.75	45.00	0.465	26.00	1.230	25.60
	86.45	52.1	45.00	0.450	24.40	1.300	24.28

TABLE 3.2 (Continued):

Cutting condition	V	F <sub>c</sub> kg	F <sub>t</sub> kg	r	$\rho$	$\mu$	$\phi_{EM}$
LN <sub>2</sub> with four nozzles	9.047	56.80	46.0	0.56	31.79	1.235	25.50
	18.025	54.37	43.0	0.601	30.10	1.206	25.80
	35.34	53.70	43.5	0.618	34.30	1.235	25.49
	45.238	52.50	42.50	0.615	34.52	1.234	25.50
	56.54	51.75	42.00	0.543	30.90	1.264	25.19
	70.685	50.00	41.50	0.4921	28.2	1.265	25.15
	90.4778	50.00	42.00	0.487	27.9	1.250	25.30
LN <sub>2</sub> with one nozzle at tip	8.641	58.71	43.00	0.65	36.32	1.1184	26.9
	13.500	54.40	41.00	0.6038	34.50	1.1510	26.49
	17.29	53.10	38.00	0.6173	3.42	1.094	27.20
	33.72	48.70	38.00	0.6307	35.30	1.189	26.70
	43.22	48.75	38.00	0.5830	32.8	1.183	26.17
	54.03	48.92	38.00	0.5940	33.40	1.985	26.10
	67.54	46.80	38.00	0.6592	36.80	1.200	25.60
	86.45	47.00	39	0.6100	34.40	1.220	55.87

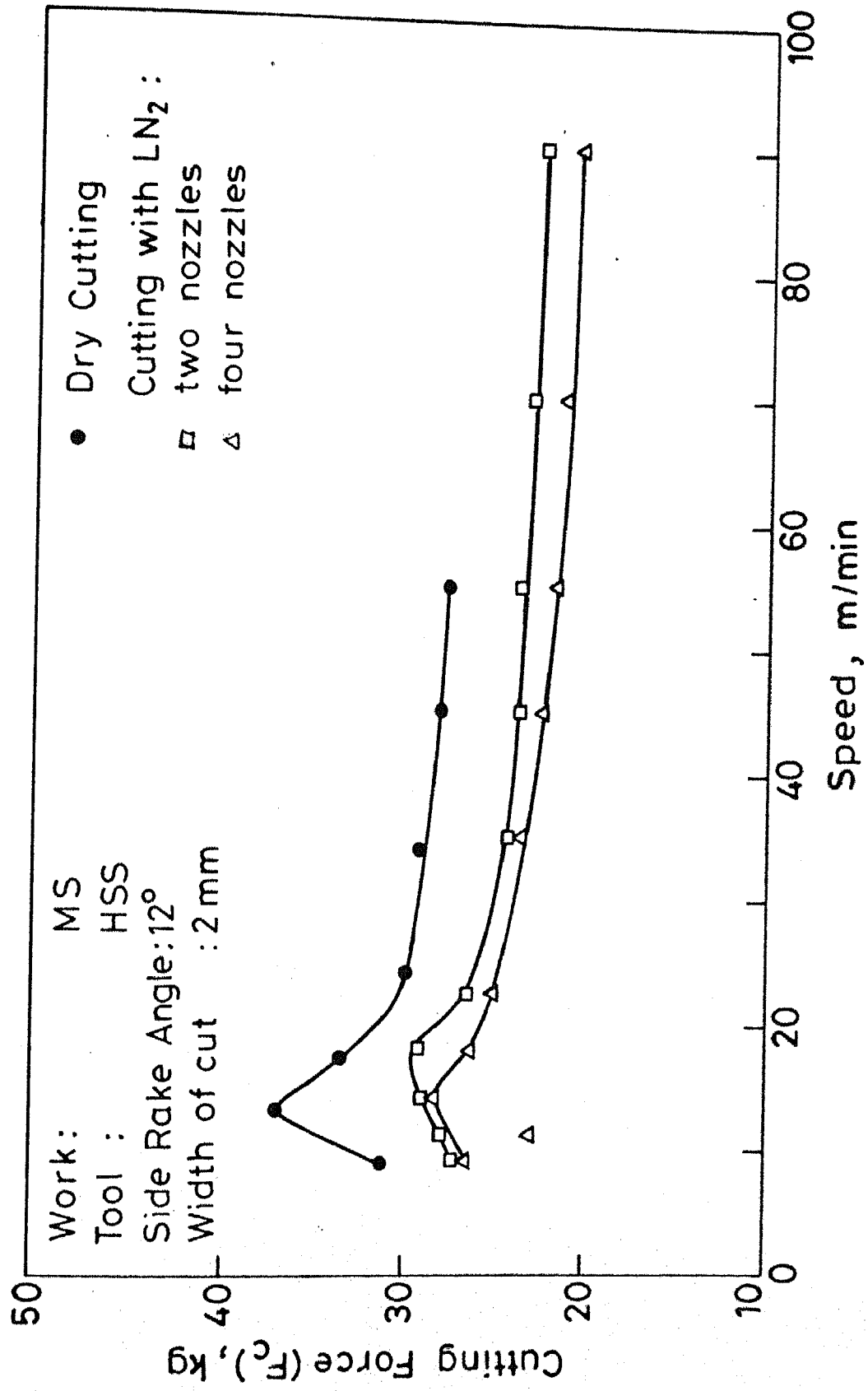


Fig.3.5 Variation of cutting force with speed (experimental).  
Feed = 0.05 mm/rev

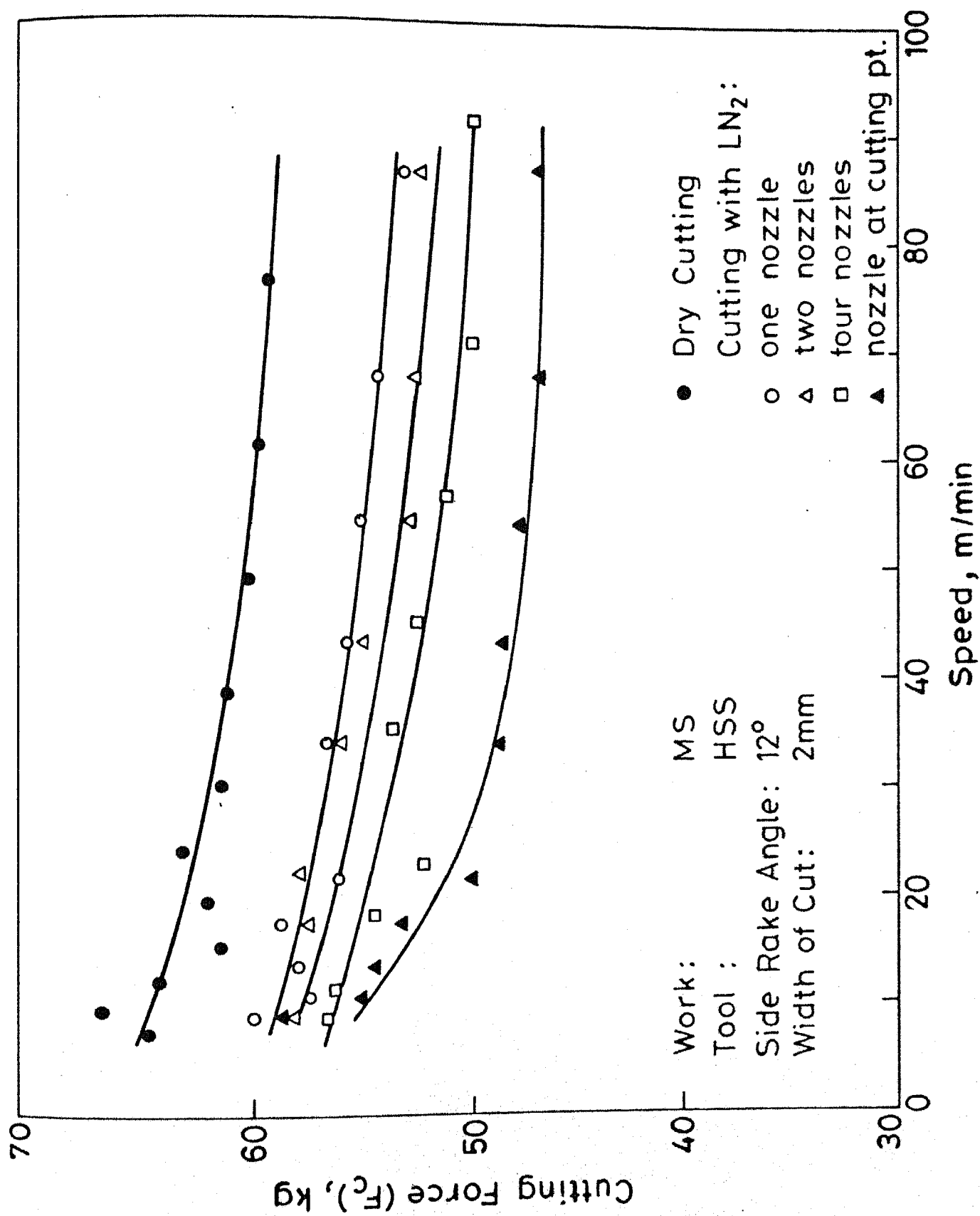


Fig.3.6 Variation of cutting force with speed (experimental). Feed = 0.125 mm/rev.

for a feed rate of .125 mm per/rev is shown. It can be seen that  $\mu$  increases with the cooling of work or <sup>with</sup> the increase in the mass flow rate of liquid nitrogen. But when liquid nitrogen was supplied just ahead the cutting tool, a significant drop in the cutting force ( $F_c$ ) as well as feed forces ( $F_t$ ) was observed. It can also be seen that in later case the mean coefficient of friction between tool and chip reduces as compared with the previous case as well as that with dry cutting.

Cutting forces ( $F_c$ ) and tool-chip interface temperature are related by the following equation:

$$\theta \propto U_c \sqrt{\frac{Vt}{k\rho c}} \quad (3.1)$$

or

$$\theta \propto \frac{F_c}{bt_f} \sqrt{\frac{Vt}{k\rho c}} \quad (3.2)$$

If experiments are conducted under identical cutting conditions (i.e. b, t and v) the interface temperature and cutting force should be related as follows:

$$\frac{\theta_2}{\theta_1} = \frac{F_{c2}}{F_{c1}} \sqrt{\frac{\rho_1 k_1 c_1}{\rho_2 k_2 c_2}} \quad (3.3)$$

where subscript 2 stands for cutting with liquid nitrogen conditions and subscript 1 stands for dry cutting condition.

From equation 3.3, we can write

$$\frac{F_{c2}}{F_{c1}} = \frac{\theta_2}{\theta_1} \sqrt{\frac{\rho_1 k_1 c_1}{\rho_2 k_2 c_2}} \quad (3.4)$$

The ratio  $F_{c2}/F_{c1}$  are calculated for various speeds (therefore for

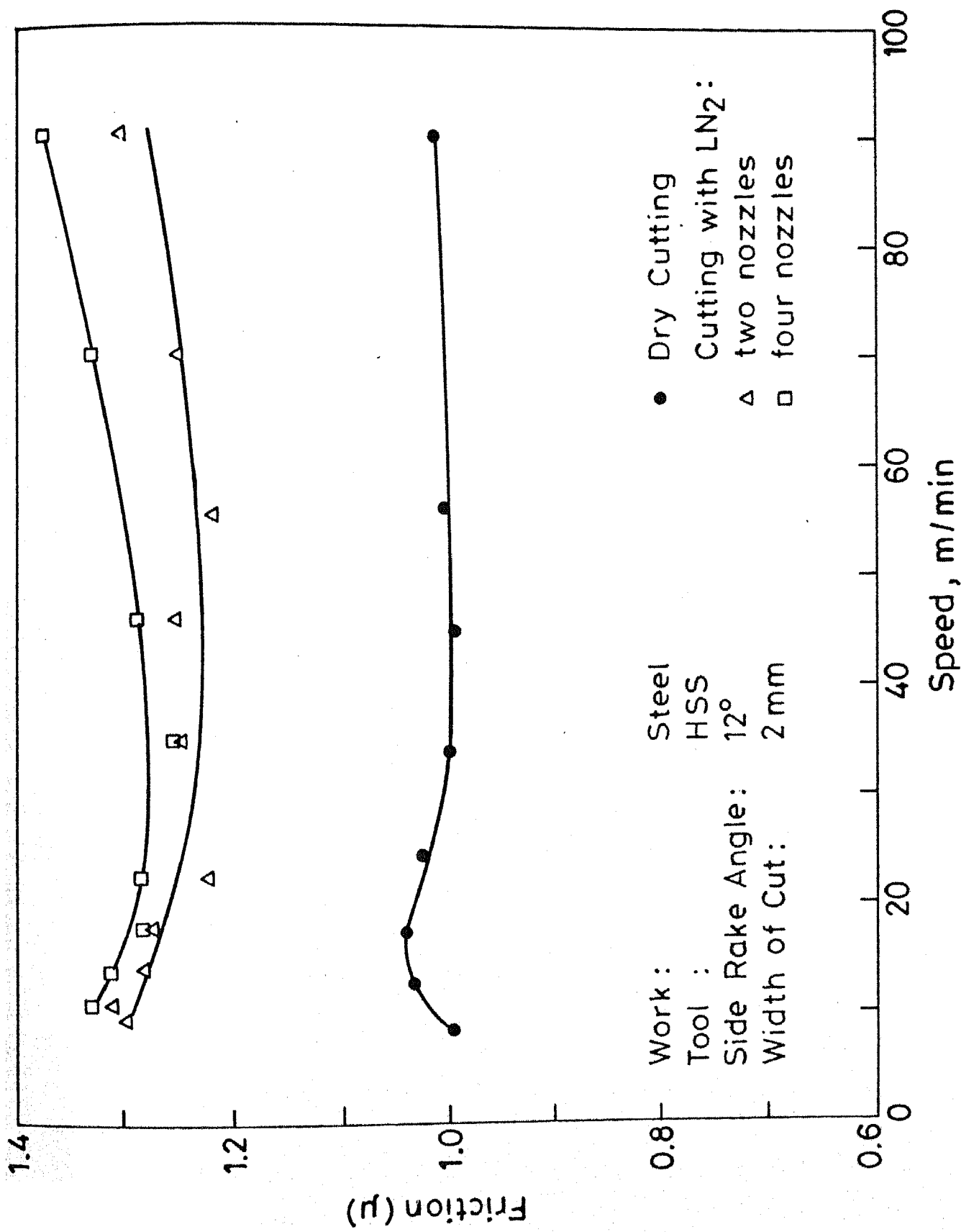


Fig.3.7 Variation of mean coefficient of friction ( $\mu$ ) with speed (experimental).  
Feed = 0.05 mm/rev

various interface temperatures) and for different mass flow rate of liquid nitrogen (different degree of cooling of workpiece) and are shown in Tables 3.3, 3.4 and 3.5. Values of  $\theta_2$  and  $\theta_1$  are taken from experimental graph (Fig. 3.2) and are entered in the columns 2 and 3 of the above tables.

The ratio of  $F_{c2}/F_{c1}$  as calculated from equation (3.4) has been compared with the ratio of the forces actually measured. The two sets of ratios of  $F_{c2}/F_{c1}$  have been entered in column 9 and 10 respectively of above tables and also plotted in Fig. 3.8. As can be seen there is a very close agreement between these two ratios. One of the conclusions which can be drawn at this stage is that change in specific cutting energy can be predicted by theoretical analysis or experimental analysis with equal accuracy.

### 3.1.3 Calculation of Maximum Tool Chip Interface Temperature

The maximum temperature rise along the tool rake face can be given as follows [Boothroyd, 28]

$$\theta_{\text{total}} = \theta_o + \theta_p + \theta_s \quad (3.5)$$

$\theta_p$  is temperature rise across the primary deformation zone, and is given by

$$\theta_p = \frac{(1 - \lambda) W_p}{\rho_c v t_1 w} \quad (3.6)$$

where  $\lambda$  is the fraction of primary heat which goes to the work piece . can be taken as follows:

TABLE 3.3 : Comparison of (Theoretical and Experimental) Cutting Force Ratio  
Using only one Nozzle

Sl. No.	Velocity m/min	Temp $\theta^{\circ}\text{C}$		$K_1$ $\times 10$	$K_2$ $\times 10$	$\rho_{1c1}$ $\times 10^5$	$\rho_{2c2}$ $\times 10^5$	$\theta_2/\theta_1$	Calcu- lated $(F_{c2}/F_{c1})$ $R_1$	Experi- mental $(F_{c2}/F_{c1})$ $R_2$	$R_2/R_1$
1.	9.75	412	377	.46	.487	.482	4.71	0.9150485	.93071	.8936651	0.960
2.	12.1	425	388	.453	.479	4.95	4.73	0.9129411	.9090	.8974358	0.987
3.	19.5	415	415	.45	.46	5	4.83	0.9325842	.92672	.8991935	0.970
4.	24.37	460	422	.44	.454	5.2	4.94	0.9173913	.9082	.888	0.978
5.	30.30	465	430	.44	.452	5.2	4.98	0.9247311	.9238	.91368	0.989
6.	38.5	472	438	.44	.451	5.2	4.99	0.9279661	.92026	.91653	0.995
7.	48.75	445	445	.43	.45	5.25	5	0.8989898	.89268	.9139	1.023
8.	60.95	515	456	.42	.444	5.35	5.1	0.8854368	.8888	.9163	1.030
9.	76.18	522	472	.41	.44	5.4	5.2	0.9042145	.9291	.9145	0.995
10.	82.00	542	477	.401	.438	5.53	5.21	0.8800738	.89552	.9059	1.011



TABLE 3.4 : Comparison of (Theoretical and Experimental) Cutting, force Ratio using only two nozzle

Sl. No.	Velocity m/min	Temperature $\theta_1$ $\theta_2$		$\theta_2/\theta_1$	$K_1$ x10	$K_2$ x10	$\rho_{c1}$ $\times 10^5$	$\rho_{c2}$ $\times 10^5$	Calculated $F_{c2}/F_{c1}$ ( $R_1$ )	Experi- men- tal $F_{c2}/F_{c1}$ ( $R_2$ )	$R_2/R_1$
1.	9.75	412	339	0.8228155	.46	.507	4.82	4.55	.83928	.8778	1.045
2.	12.1	425	355	0.8352941	.453	.495	4.95	4.61	.84263	.897	1.06
3.	19.5	445	381	0.8561797	.45	.485	5.00	4.71	.86268	.931	1.07
4.	24.37	460	390	0.847826	.44	.479	5.2	4.74	.84456	.908731	1.07
5.	30.3	465	401	0.8623655	.44	.472	5.2	4.76	.8689	.91012	1.0543
6.	38.5	472	405	0.8580508	.44	.47	5.2	4.78	.86405	.9083469	1.0512
7.	48.75	495	411	0.830303	.43	.465	5.25	4.82	.83528	.88916	1.0645
8.	60.95	515	420	0.8155339	.42	.454	5.35	4.93	.813935	.8918	1.0956
9.	76.18	522	433	0.8295019	.41	.452	5.4	4.985	.8368	.89743	1.072
10.	82.00	542	440	0.8118081	.401	.451	5.53	4.992	.81814	.8931	1.0916

TABLE 35 : Comparison of (Theoretical and Experimental) cutting Force Ratio Using only Four Nozzle

Sl. No.	Velocity m/min	Temperature $\theta_1$	$\theta_2$	$\theta_2/\theta_1$	$k_1$ $\times 10$	$k_2$ $\times 10$	$\rho_{1c1}$ $\times 10^5$	$\rho_{2c2}$ $\times 10^5$	Calculated $F_{c2}/F_{c1}$ ( $R_1$ )	Experimental $F_{c2}/F_{c1}$ ( $R_2$ )	$(R_2/R_1)$
1.	9.75	412	310	0.7524271	.46	.515	4.82	4.42	.76236	.852187	1.1178
2.	12.10	425	324	0.7623529	.453	.51	4.95	4.52	.77295	.866000	1.1200
3.	19.50	445	352	0.7910112	.45	.494	5.00	4.60	.79493	.870000	1.0900
4.	24.37	460	360	0.7826086	.44	.492	5.20	4.63	.78088	.834000	1.0600
5.	30.30	465	369	0.7935483	.44	.491	5.20	4.69	.796108	.863192	1.0800
6.	38.50	472	380	0.8050847	.44	.485	5.20	4.716	.80494	.8756	1.0878
7.	48.75	495	387	0.7818181	.43	.480	5.25	4.728	.78387	.860215	1.0970
8.	60.95	515	399	0.7747572	.42	.473	5.35	4.77	.77633	.8579885	1.1000
9.	76.18	522	409	0.7796934	.41	.469	5.40	4.78	.78457	.8540000	1.0800
10.	82.00	542	410	0.7564575	.401	.466	5.53	4.79	.75894	.8540000	1.1200

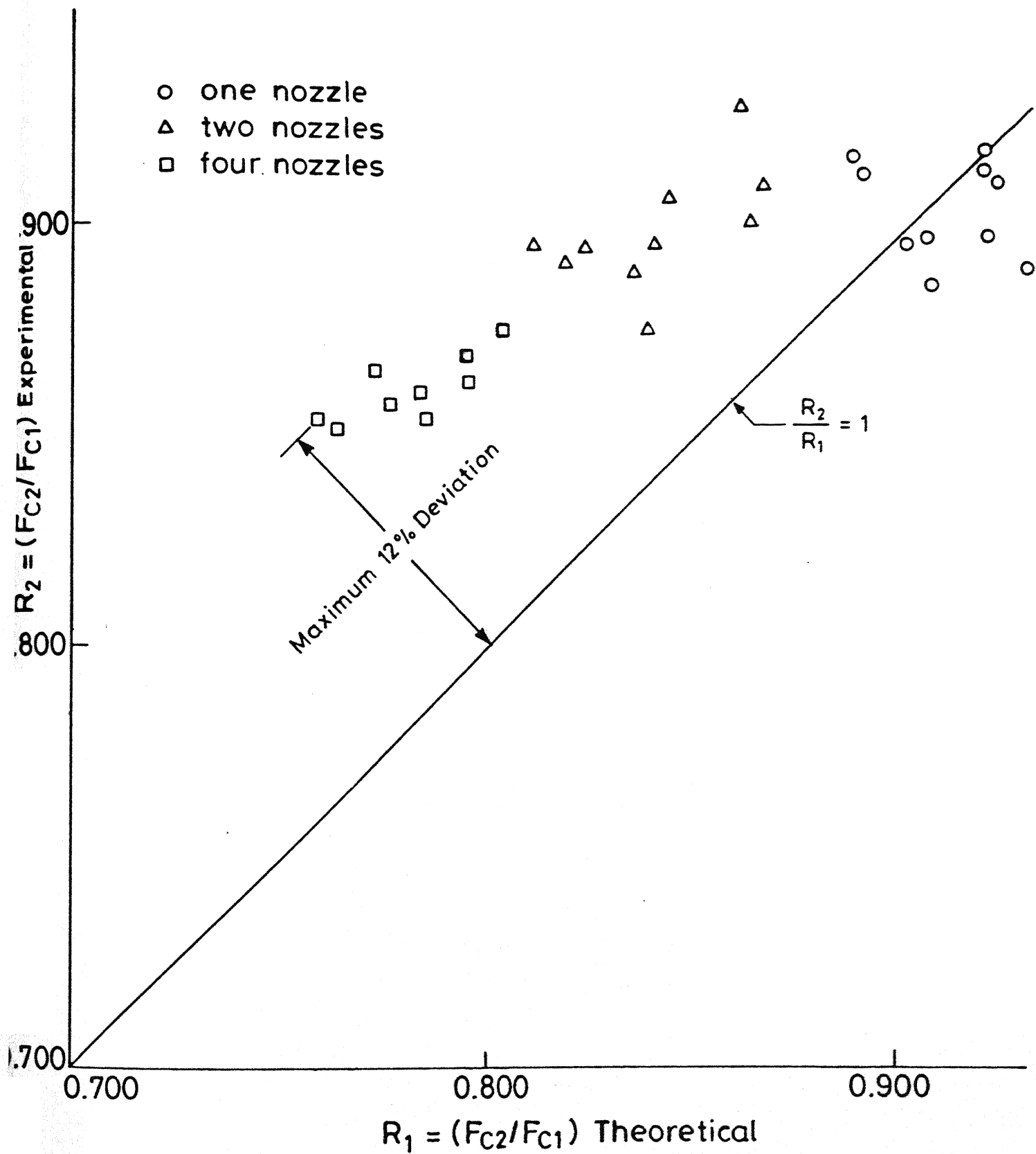


Fig. 3.8 Comparison of (theoretically and experimentally) cutting ratio.

$$\lambda = .15 \ln \left( \frac{27.5}{\tan \phi, \Theta} \right) \quad (3.7)$$

where

$$\Theta = \frac{\rho_c v t_1}{k}$$

$\Theta_s$  is temperature rise along the rake face of the tool through the secondary deformation zone and is given by

$$\Theta_s = 1.13 \sqrt{\frac{\Theta t_2}{1}} \left( \frac{W_s}{\rho_c v b t_1} \right) \quad (3.8)$$

where

$$\frac{1}{t_2} = 1 + \tan(\phi - \alpha)$$

The following assumptions were made while deriving the above equations:

- (1) All of the energy expended at shear zone and along the tool face are converted to thermal energy.
- (2) The energy at shear zone and at along the tool face is concentrated on a plane surface .
- (3) Energy at shear zone and along the tool face is uniformly distributed.

In order to calculate  $\Theta_{total}$  the following calculations are necessary:

- (i) Calculation of chip thickness ratio, 'r'
- (ii) Calculation of shear plane angle, ' $\phi$ '
- (iii) Calculation of fraction of heat generated at shear zone which goes to workpiece, ' $\lambda$ '
- (iv) Calculation of plastic deformation work at primary deformation zone ( $W_p$ ), and secondary deformation zone ( $W_s$ ).

(i) Calculation of 'r'

The chip thickness ratio,  $r$ , is defined as the ratio of uncut chip thickness to the chip thickness. This is calculated by measuring the weight and length of collected chips

$$r = \frac{t_1}{t_2}$$

where

$$t_2 = \frac{W}{l_2 \times b \times \rho}$$

values of  $r$  for known values of feed rate  $t_1$  and width of cut  $b$  were estimated and these values have been entered in column 5 of Tables 3.1 and 3.2. The variation of  $r$  with speed is conventionally a decreasing function with speed. However, present experiments did not always yield this trend. Conventionally observed trend has been observed only in lower speed but not in higher speed. The agreement between the conventionally observed and the measured values of  $r$  in present work has been found to be better at lower feed than at higher feed.

It is possible that at the higher speed the stability of dynamometer which was holding the cutting tool was not good. Also a simple calculation shows that the 2% error in the pitch of lead screw can cause about 25% error in the estimation of the chip thickness ratio. If one has to measure  $r$  very accurately a steady lathe with a lead screw of negligible backlash and excellent dynamometer mounting is required.

(ii) Calculation of Shear Angle ' $\phi$ '

Shear plane angle can be estimated either using simple shear plane model or from one of the standardised shear plane equations based on Ernest and Merchant, Lee and Shaffer or other similar equations. The values of  $\phi$  calculated on the basis of simple shear plane models incorporate the values of  $r$  as shown by the following equation:

$$\tan \phi = \frac{r \cos \alpha}{1 - r \sin \alpha} \quad (3.9)$$

Ernest and Merchant formula has also been used to calculate the value of  $\phi$ .

$$2\phi + \beta - \alpha = \frac{\pi}{2} \quad (3.10)$$

In order to calculate the value of  $\phi$  from above equation, value of friction coefficient  $\mu$  has been calculated from the following equation:

$$\mu = \tan \beta = \tan^{-1} (F/N) \quad (3.11)$$

where

$$F = F_c \sin \alpha + F_t \cos \alpha$$

and

$$N = F_c \cos \alpha - F_t \sin \alpha$$

In this equation  $F_c$  and  $F_t$  represent the cutting forces respectively which were recorded by dynamometers.

The value of  $\phi$  calculated by using equations (3.9) and (3.10) have been presented in columns 6 and 8 in Tables 3.1 and Table 3.2. It is interesting to observe that two sets of  $\phi$  values are within 15 to 20% variation under dry cutting conditions. Under liquid nitrogen conditions the maximum observed order of mismatch is 25%.

Some authors have recommended to use Lee and Shaffer equation for the estimation of  $\phi$ . In present case, the use of Lee and Shaffer equation gives a mismatch of large magnitude (approximately 50%). Therefore the Ernest and Merchant solution was observed to be better applicable for larger values of coefficient of friction (more than unity) in the present experiments. However the shear plane model (eqn. 3.9) was chosen for the calculation of  $\phi$  values in the present work, as it involves only one experimentation.

### (iii) Calculation of ' $\lambda$ '

Equation (3.7) shows the expression for  $\lambda$ . Normally an iterative method is used to calculate the value of  $\lambda$  when accurate temperatures estimations are required. Since in the present work the objective was to compare the two situations

(dry cutting and liquid nitrogen cutting) a simple though little less accurate method was used to estimate the value of  $\lambda$ .  $\lambda$  was calculated under room temperature properties, and this was used to calculate  $\Theta_p$ . For subsequent actual calculation of  $\lambda$  thermal properties were taken at  $\Theta_p$ .

(iv) Calculation of  $W_p$  and  $W_s$

$W_p$  and  $W_s$  are given by

$$W_p = F_c.V - F_r.V$$

and  $W_s = F_r.V$  respectively

where  $F$  is equal to

$$F = F_c \sin \alpha + F_t \cos \alpha$$

$F_c$  and  $F_t$  are measured by dynamometers.  $V$  is cutting velocity and calculation of  $r$  has already been explained earlier. Thus the rate of heat generation in primary zone ( $W_p$ ) and the secondary zone ( $W_s$ ) can be found.

The estimate of these quantities have been presented in the columns of 2 and 3 respectively of Tables 3.6, 3.7, 3.8 and 3.9.

It is very interesting to observe that when  $\Theta_p$  is calculated from equation (3.4) and  $\Theta_s$  from equation (3.6) the final maximum temperature  $\Theta$  agrees quite well with the temperature measured by using tool work thermocouple technique.

This can be seen from Tables 3.6 to 3.9 and variation



TABLE 3.6 : Comparison of (Theoretical and Experimental) Tool-chip Interface Temperature when Machining MS in Dry Cutting Condition

$t = .125$  mm/rev.

$k = 54$  W/m°C

$c = 500$  J/kg°C

$\rho = 7800$  kg/m<sup>2</sup>

S.No.	V m/min	$\lambda$	$W_p$ (Nm/s)	$W_s$	$\theta_p$ °C	$\theta_s$ °C	$\theta_{total}$ °C	$\theta_{experiment}$ °C
1.	9.75	.5123	54.58	51.11	168.0	221.80	419	412
2.	19.50	.3853	97.56	100.10	189.2	217.93	437	445
3.	38.5	.3318	216.3	168.6	231.0	207.76	468	472
4.	60	.2914	376.18	204.08	278.39	186	494	515
5.	72	.2480	467.64	259.94	286.60	187.35	503	522

TABLE 3.7 : Comparison of (Theoretical and Experimental) Tool Chip Interface Temperature when Machining MS using only one Nozzle

$\rho = 7800 \text{ kg/m}^3$

$c = 499 \text{ W/m}^\circ\text{C}$

S.No.	V m/min	$\lambda$	$W_p$	$W_s$ (Nm/s)	$\theta_p$ $^\circ\text{C}$	$\theta_s$ $^\circ\text{C}$	$\theta_{\text{total}}$ $^\circ\text{C}$	$\theta_{\text{experimental}}$ $^\circ\text{C}$
1.	8.64	.534394	39.76	44.99	132.08	209.9	371.9	365
2.	13.50	.46195	58.58	69.716	143.96	207.50	381.46	390
3.	17.29	.429307	77.13	88.95	156.95	208.319	395.26	405
4.	33.72	.322493	134.82	175.29	167.03	209.405	406.40	427
5.	43.22	.30349	193.74	199.32	192.52	199.98	422.5	440
6.	54.03	.27496	246.70	239.16	204.13	197.12	431.29	450
7.	67.54	.24750	312.40	288.05	224.62	194.86	449.48	465
8.	86.45	.21570	396.15	349.49	24.586	190.853	462.43	475

TABLE 3.8 Comparison of (Theoretical and Experimental) Tool-chip Interface Temperature with two Nozzles  $k = 53 \text{ W/m}^2\text{C}; \rho = 7800 \text{ Kg/m}^3; c = 498 \text{ W/m}^2\text{C}$

Sl.No.	$V$ m/min	$\lambda$	$W_p$	$W_s$ ( $N_m/s$ )	$\theta_{Cp}$ $^{\circ}\text{C}$	$\theta_{Cs}$ $^{\circ}\text{C}$	$\theta_{total}$	$\theta_{experimental}$
1.	8.64	.53675	39.403	42.708	130.00	217.16	377.00 $^{\circ}\text{C}$	330 $^{\circ}\text{C}$
2.	13.50	.45568	55.542	69.71	138.36	208.74	377.10 $^{\circ}\text{C}$	355 $^{\circ}\text{C}$
3.	17.29	.42030	70.67	91.878	146.39	211.70	388.09 $^{\circ}\text{C}$	368 $^{\circ}\text{C}$
4.	33.72	.31952	129.81	178.923	161.85	211.89	403.74 $^{\circ}\text{C}$	395 $^{\circ}\text{C}$
5.	43.22	.2945	180.23	208.424	181.77	205.09	417.06 $^{\circ}\text{C}$	405 $^{\circ}\text{C}$
6.	54.03	.2744	231.26	234.724	191.89	197.70	419.59 $^{\circ}\text{C}$	415 $^{\circ}\text{C}$
7.	67.54	.24067	283.77	298.73	197.134	129.00	426.00 $^{\circ}\text{C}$	422 $^{\circ}\text{C}$
8.	86.456	.20439	372.39	364.43	211.97	195.00	436.04 $^{\circ}\text{C}$	440 $^{\circ}\text{C}$

TABLE 3.9 : Comparison of (Theoretical and Experimental) Tool Chip Interface Temperature when Machining MS Using only Four Nozzles  
t = 125 mm

k = 52 W/m°C

$\rho$  = 7800 kg/m<sup>3</sup>

c = 495 J/kg/m<sup>2</sup>

S.No.	V m/min	$\lambda$	$W_p$ (Nm/s)	$W_s$	$\theta_p$ °C	$\theta_s$ °C	$\theta_{total}$	$\theta_{experimental}$
1.	9.047	.52	30.964	47.05	121.9	208.38	324°C	300°C
2.	18.095	.4029	65.12	94.9	133.57	186	349.57°C	345°C
3.	35.34	.3	190.96	189.32	148.93	188.60	366°C	370°C
4.	45.238	.2651	153.477	234.83	154.74	184.80	368°C	383°C
5.	56.54	.2488	214.56	259.70	176.78	178.60	385°C	395°C
6.	70.685	.2308	287	290.00	194.42	172.26	395°C	405°C
7.	90.4778	.1470	354.8	370.9	201.25	172.2	403°C	410°C

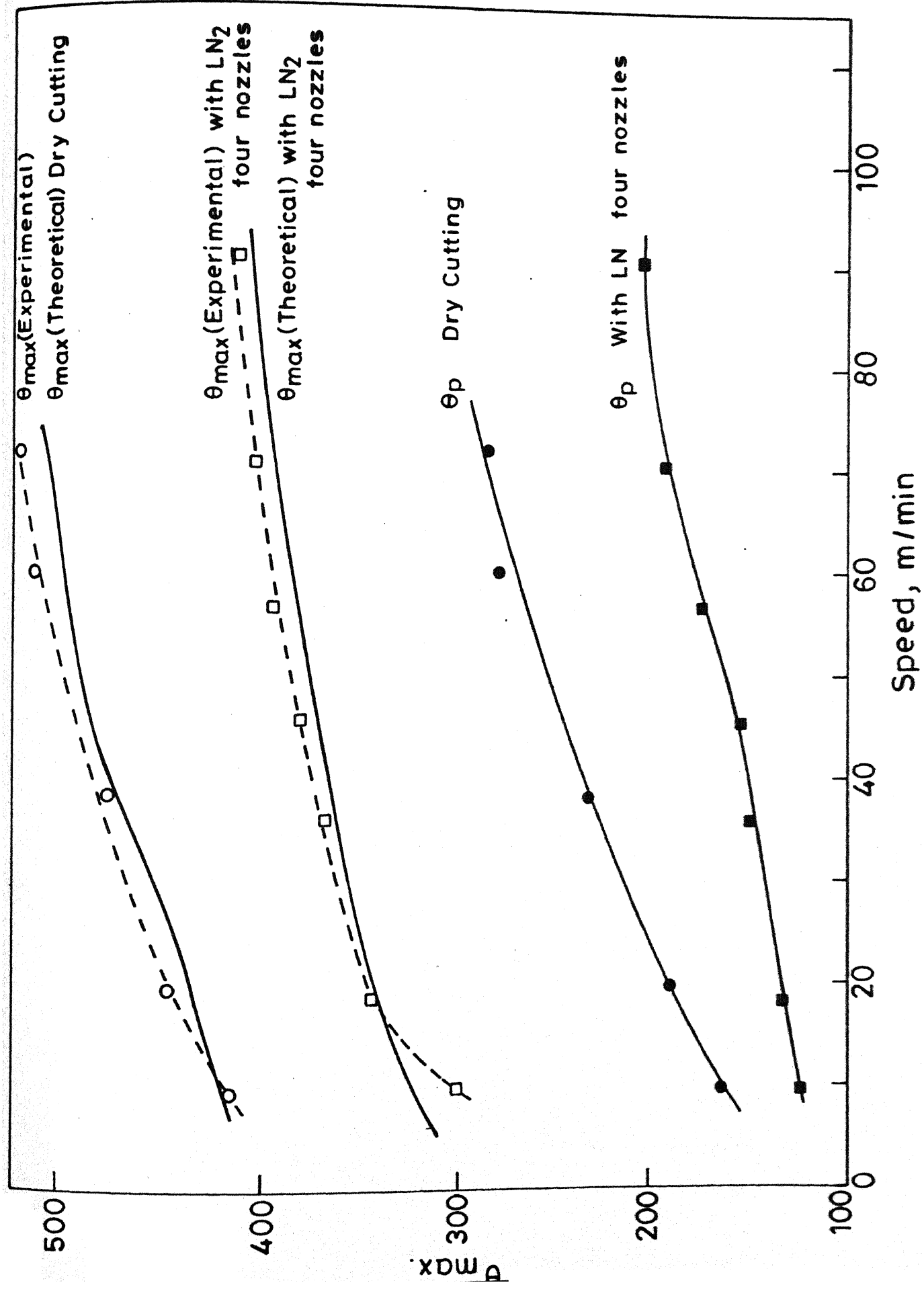


Fig. 3.9 Comparison of (theoretical and experimental) max. tool chip interface temp.

of  $\theta_{total}$  (theoretical and experimental) with velocity is plotted in Fig. 3.9.

Figure 3.10 shows variation of heat partition factor with  $(\frac{v \tan \phi \rho_{ct1}}{k})$  when this figure is compared with the Fig. (3.11) [Boothroyd, 28] it is seen that there is quite a good similarity between them. Curve 3.11 is valid for various materials under different combination of cutting conditions of  $v$ ,  $\phi$  and  $t_1$  whereas present curves confirms that the influence of liquid nitrogen has change the mechanical properties of material as a result of cooling without changing the mechanism of cutting. However when the liquid nitrogen jet was impinged just ahead of the cutting edge, factor  $\lambda$  decreased and this is seen the change, the influence mechanism of cutting indeed the values of coefficient of friction decreased (Table 3.2) this indication that the mechanism of chip formation changed, it was also observed that the chip obtained were thinnest.

It is to be observed that equation (3.1) has been obtained by dimensional analysis approach whereas equation (3.6) and (3.8) have been obtained on the analysis of temperature in the deformation zones.

Using both these approaches in the present work it can be seen that <sup>there</sup> is fairly good agreement between theoretical and experimental work both for temperature as well as forces exist. It confirms that the mechanism of temperature generation and mechanism of cutting for steel in dry condition and liquid nitrogen condition are similar.

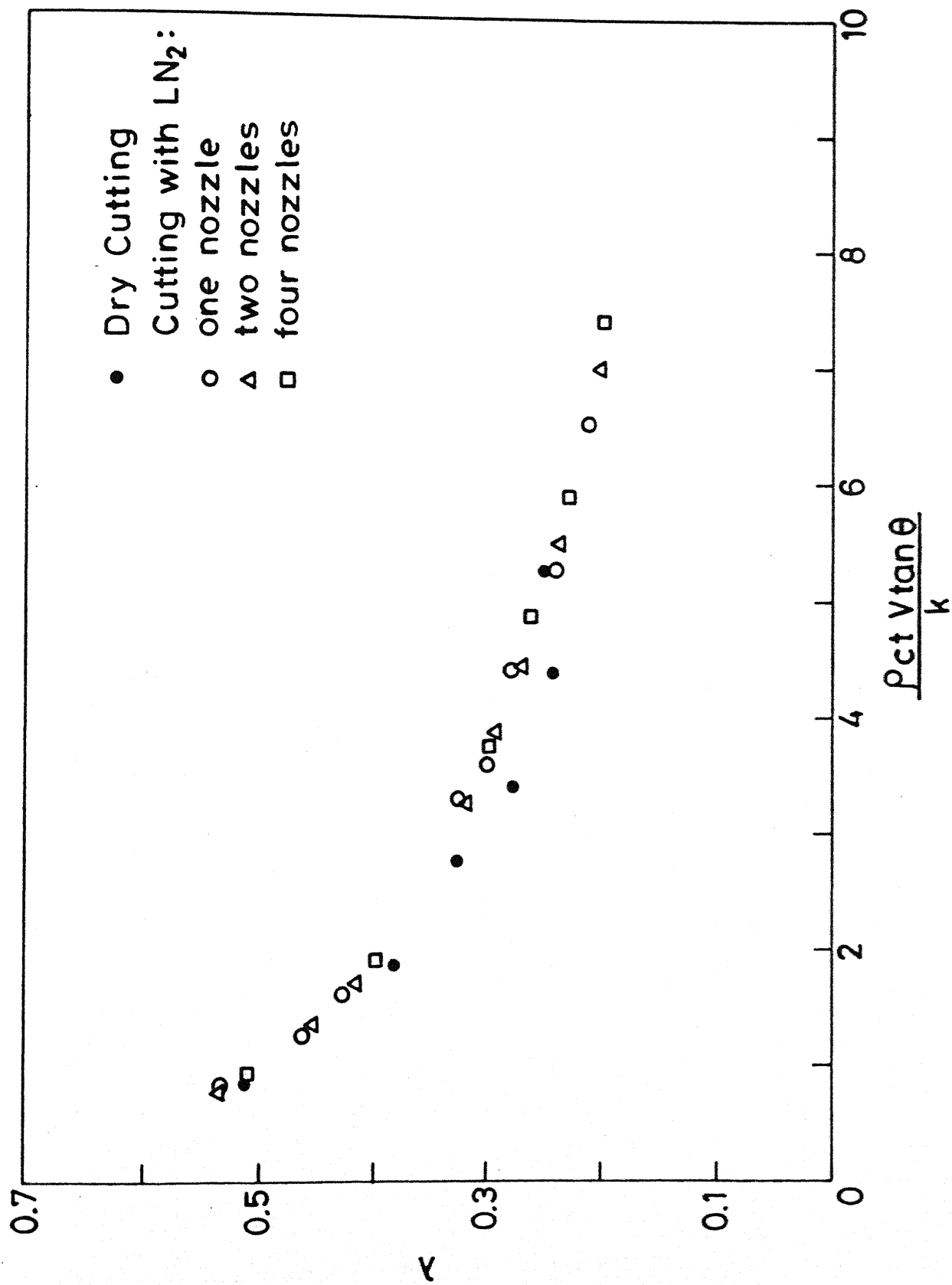


Fig.3.10 Variation of heat partitioning factor with cutting condition.

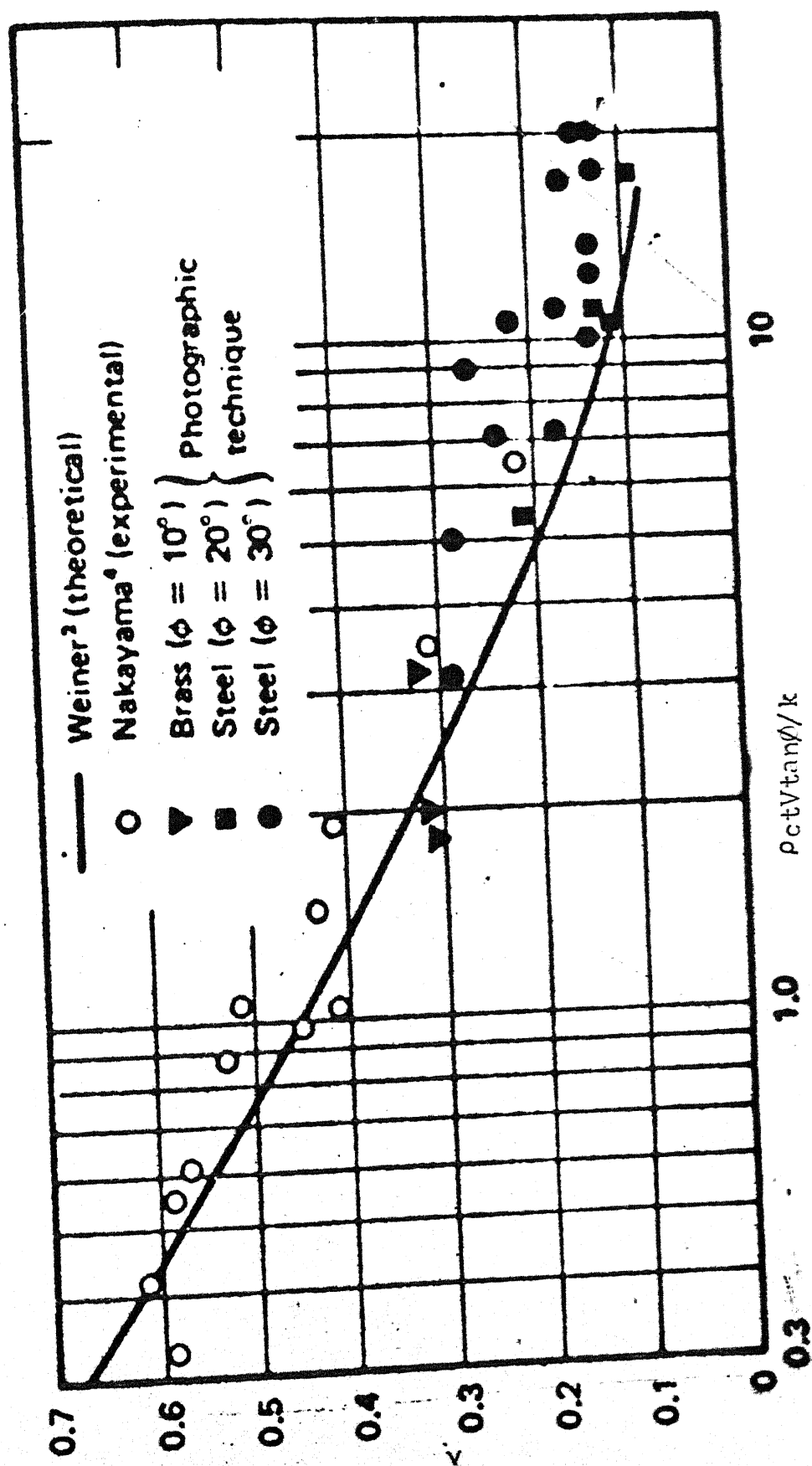


Fig.3.11 : Effect of  $\rho ct V \tan \phi / k$  on division of shear heat between chip and workpiece, where  $\lambda =$  the proportion of shear zone heat conducted into the workpiece (After Boothroyd 28)



### 3.2 Machining of Titanium

Figures 3.12, 3.13 show the variation of temperature at various speeds and Figs. 3.15, 3.16 show the variation of cutting force  $F_c$  at corresponding speeds.

#### 3.2.1 Cutting Temperature

Figures (3.12) and (3.13) give the variation of temperature for two different feeds with and without liquid nitrogen. It can be seen that the fall in temperature obtained is very significant in both the cases. It can also be seen from Fig. 3.4 and Fig. 3.14 that the percentage fall in temperature reduces with increase in speed. For feed .125 mm/rev., the percentage fall with speed <sup>is</sup> sharp and reduces continuously whereas percentage reduction in temperature with feed .05 mm/rev. is of higher magnitude and reduces sharply at the beginning then at higher speeds reduces slowly. For the same value of temperature of dry cutting at two different feed, the percentage drop in temperature is higher for the feed of .05 mm/rev.

Temperature is also calculated theoretically based on shear plane theory (Table 3.10) as it was calculated for mild steel in section (3.13). In this case, there seems to be almost no agreement between the temperature theoretically calculated and experimental obtained. It can be concluded from that

(a) chip formation mechanism is different than continuous chip formation, so above calculation are not valid for Titanium alloys.

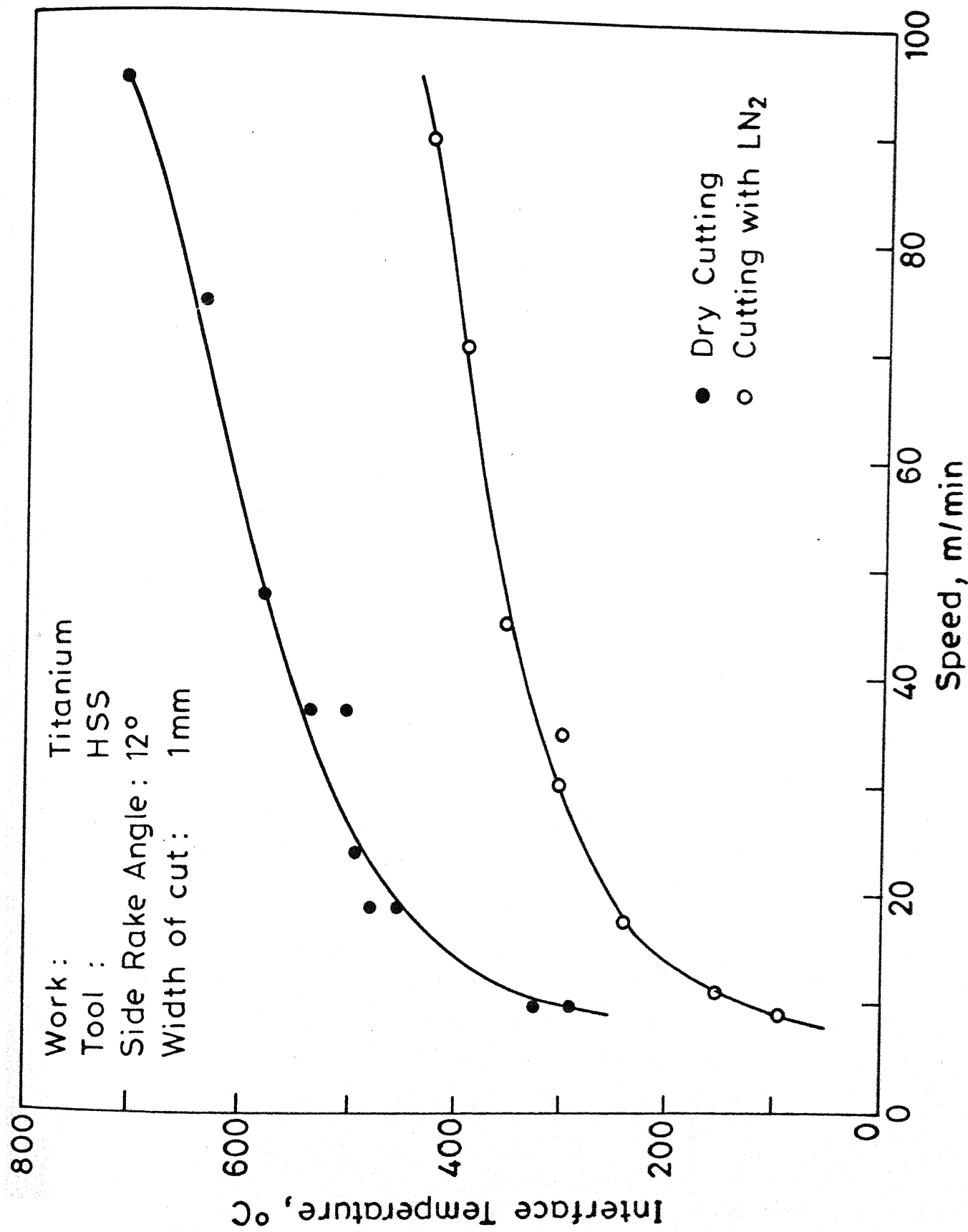


Fig.3.12 Variation of interface temperature with speed (experimental).  
Feed = 0.05 mm/rev .

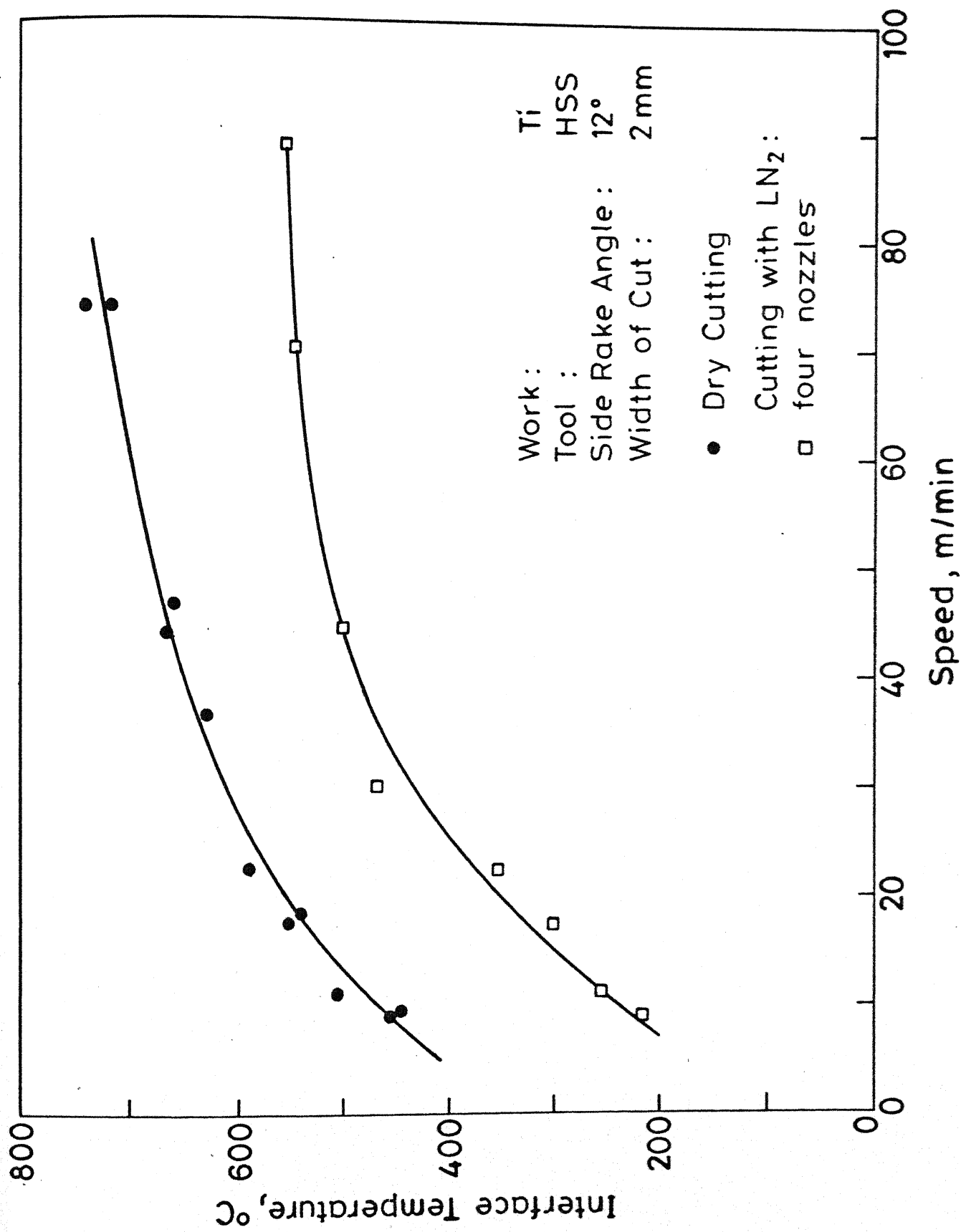


Fig.3.13 Variation of interface temperature with speed. Feed = 0.125 mm/rev

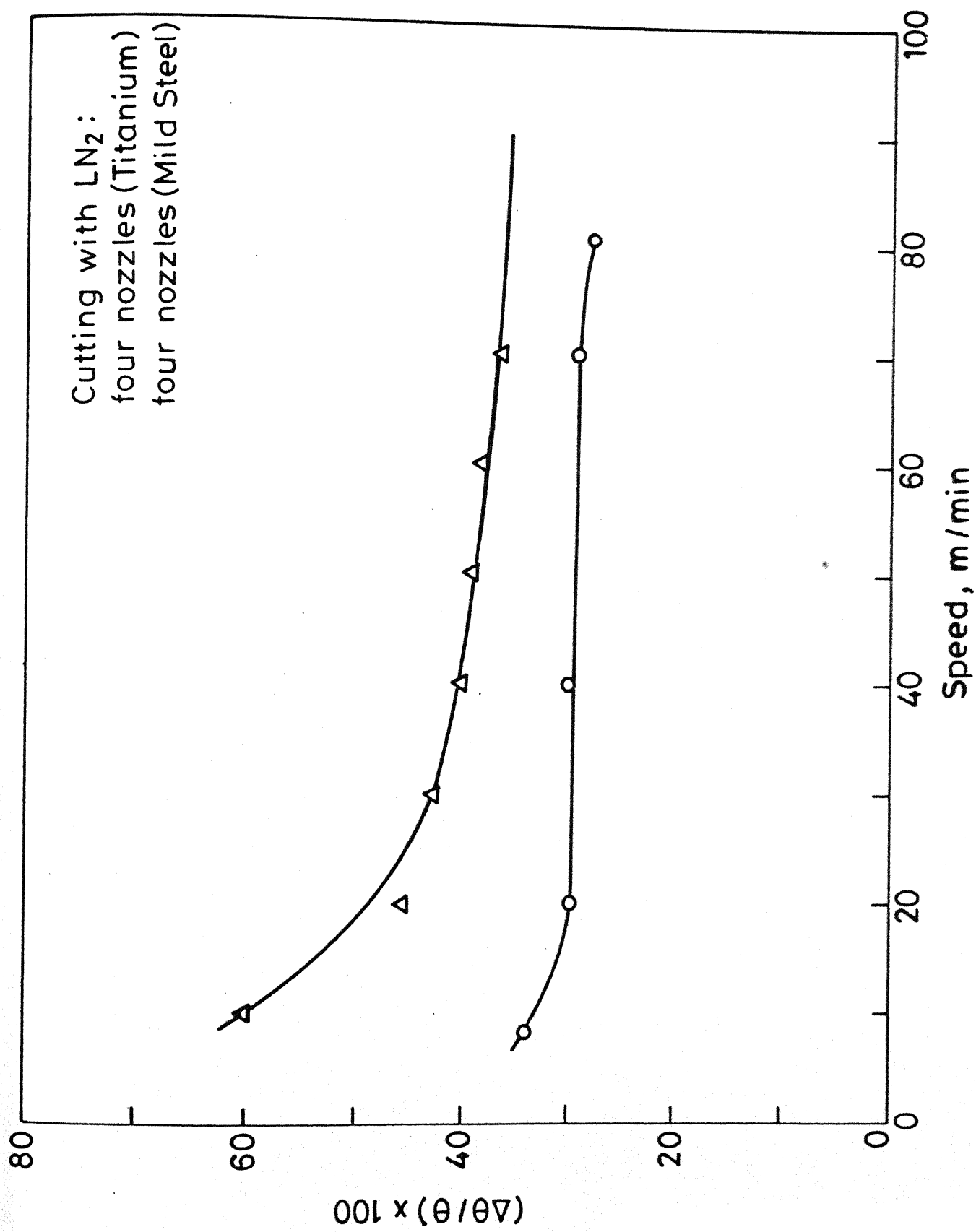


Fig.3.14 Percentage variation in temperature with speed. Feed=0.05mm/rev

TABLE 3.10 : Comparison of (Theoretical and Experimental) Tool Chip Interface Temperature when machining titanium

V m/min	r	$\phi$	$\mu$	$\phi_{EM}$	$\lambda$	$W_P$ $\frac{Nm}{Sec}$	$N_C$ $\frac{Nm}{Sec}$	$\theta_p$ $^{\circ}C$	$\theta_s$ $^{\circ}C$	$\theta_{total}$ calculated $^{\circ}C$	$\theta_{experimental}$
<u>Dry cutting</u>											
7.9	.417	29.462	1.50	28.5	.38	24.1	18.28	240.0	258.00	527.0	505
22.2	.463	26.669	0.91	29.82	.292	48.4	27.04	274.69	248.2	55.2	595
44.4	.515	29.462	0.83	31.50	.171	91.1	54.00	302.80	243.00	515.0	675
69.4	.525	29.96	0.8109	31.09	.10	142.0	84.20	327.60	241.86	599.4	715
<u>With liquid nitrogen</u>											
22.2	.595	33.62	0.9447	29.31	.250	37.2	34.2	223.40	265.48	518.80	385
69.4	.654	36.52	1.057	27.70	.063	01.6	106.4	229.8	259.2	508.6	525
88.5	.6522	36.43	0.9620	22.05	.022	114.0	130.5	223.9	254.0	507.25	580

or

(b) Even if the mechanism of continuous chip formation is applicable, there must be some other source of heat generation other than in the shear zone and along the tool face or both (a) and (b).

### 3.2.2 Cutting Force

As can be seen from Fig. (3.15) and Fig. (3.16) drop in forces with liquid nitrogen is very small, almost negligible, as compared to the fall in forces with mild steel. Also calculating from Table 3.11 show that the specific cutting energy for Titanium falls by 5% only under liquid nitrogen condition whereas for the mild steel the decrease was nearly 15% in same speed range. The exact importance of this features could be discussed here if the two work pieces used were identical. Generally the variation in specific cutting energy is considered, be due to the material property, this may also have connecting with microstructure, the level of defect density and lattice structure.

The author can only think that it is atomsitic features which have to be investigated in depth to establish the reason for above differences in specific cutting energy.

The calculation made in section 3.1.2 for mild steel for different temperatures were repeated for the case of Titanium to calculate the ratio of forces as shown in Table 3.12. This table show that the agreement between the relations of  $F_{c2}/F_{c1}$  (experimental) is almost absent. Which shows quite a different trend than that seen in the cutting of mild steel. Accordingly

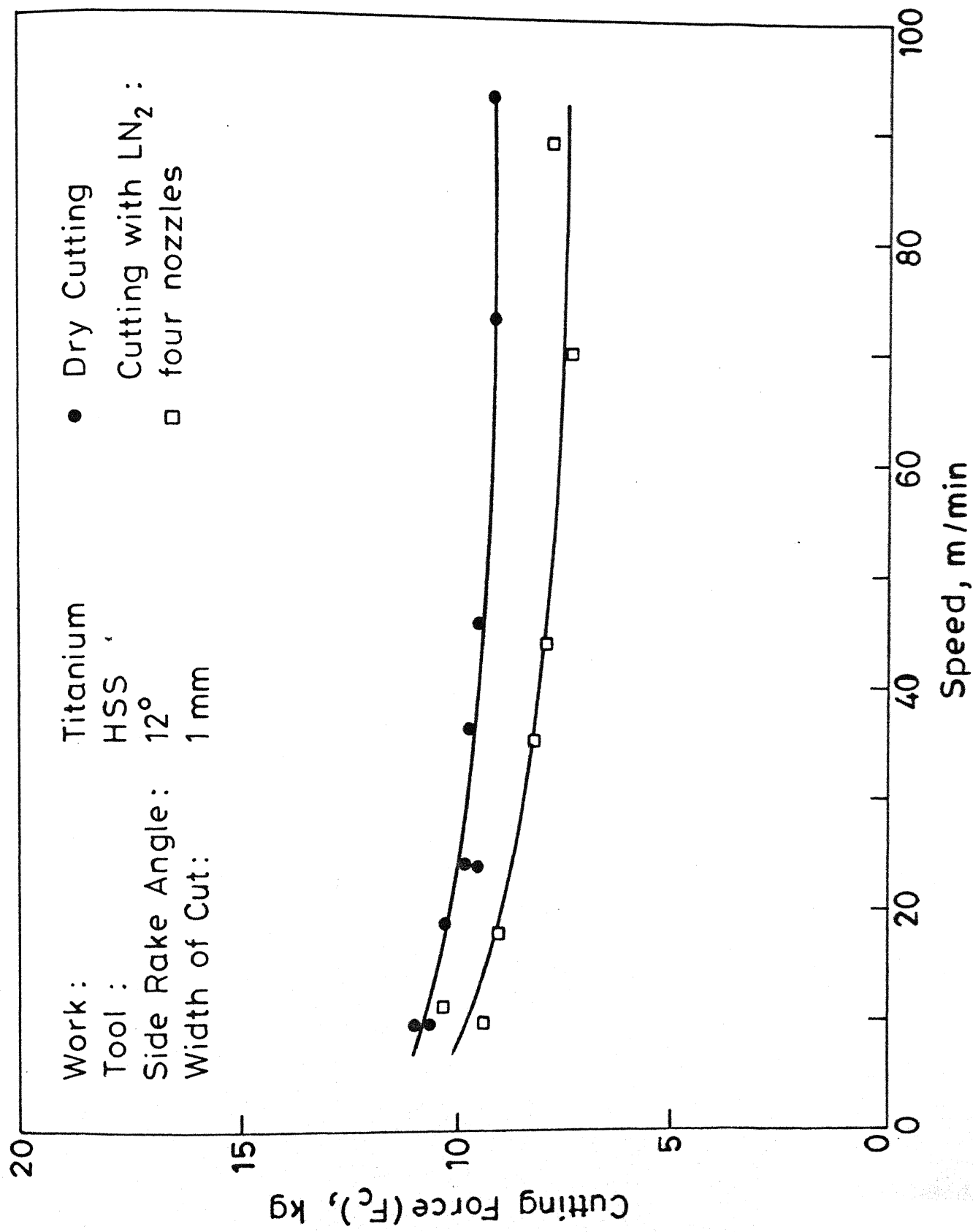


Fig.3.15 Variation of cutting force with speed (experimental). Feed = 0.05 mm/rev

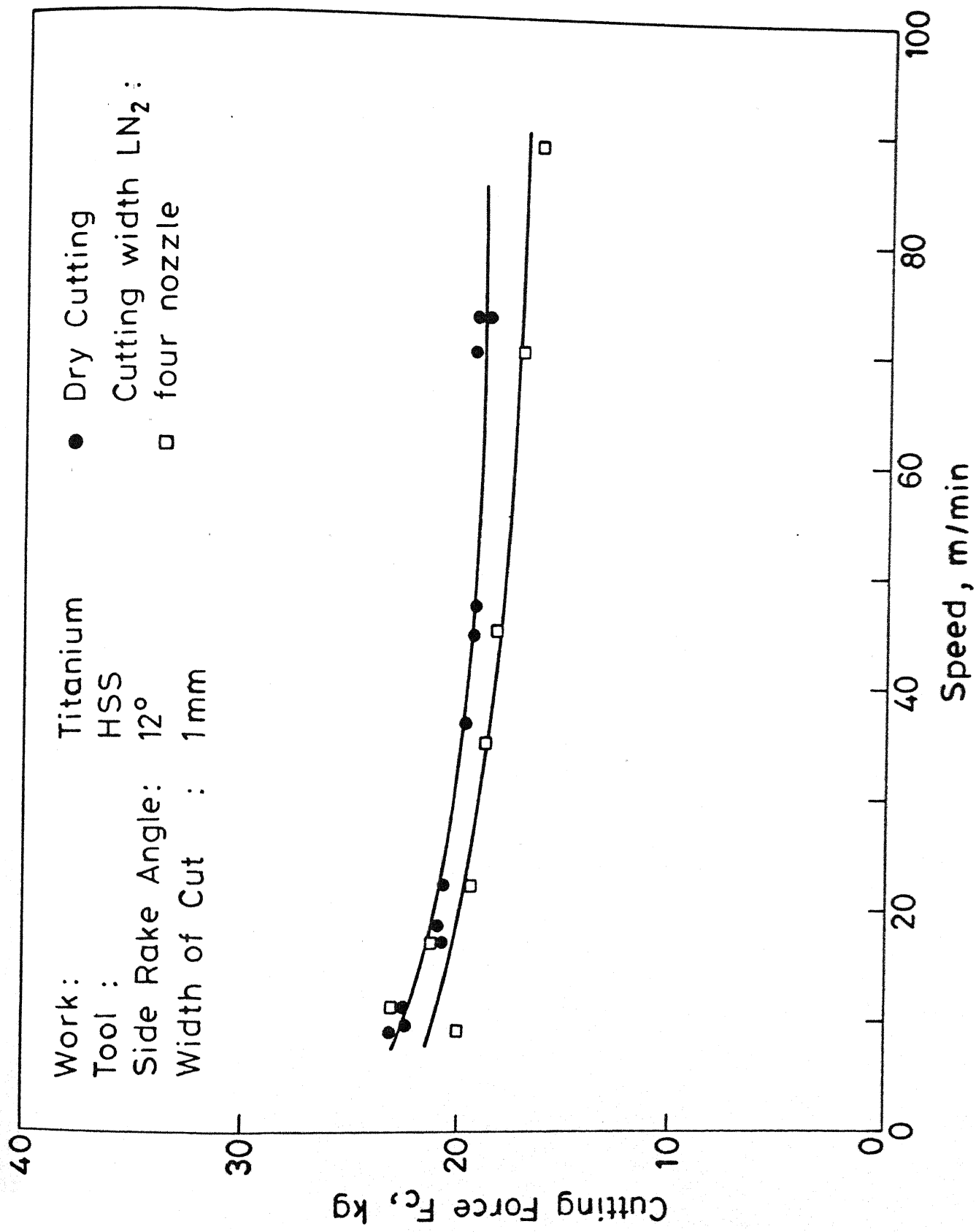


Fig.3.16 Variation of cutting force with speed (experimental). Feed = 0.125 mm/rev



TABLE 3.11: Comparison of Specific Cutting Energy  
Feed =  $t = .125$  mm/rev.

Work - Titanium, $b = 1$ mm					Work - MS, $b = 2$ mm				
V	$F_c$	$F_c$	$F_c$	$\frac{F_c}{bt}$	V	$F_c$	$F_c$	$F_c$	$\frac{F_c}{bt}$
m/min	dry	(LN <sub>2</sub> )	Dry	LN <sub>2</sub>	m/min	kg	kg	Dry	LN <sub>2</sub>
9	23.4	20.9	187	167.5	7	65	56.8	260	227
11	22.75	23.1	182	185.0	10	65	56.2	260	225
17.3	20.80	21.2	166.4	169.4	18	61.4	54.3	245.6	217.2
22.2	20.8	19.6	166.4	152.8	25	63	52.5	252.0	210.0
69.4	91.0	17.5	168.0	140.0	38	60.5	50.0	242.0	200.0
			171.0	161.0				252.0	215.0

% reduction in specific energy

$$= \frac{171-161}{171} \times 100 = 5\%$$

% reduction in specific energy

$$\frac{252-215}{252} \times 100 = 14.6\%$$

TABLE 3.12: Comparison of (Theoretical and Experimental) Force Ratio when Cutting Titanium using four Nozzles

Sl. No.	Velocity	$\theta_1$	$\theta_2$	J kg/°C		$F_{c2} / F_{c1}$	$F_{c2}/F_{c1}$		$(R_2/R_1)$
				$c_1$	$c_2$	Theoretical	Experimental	Experimental	
1.	8.9	450°C	250	621.4	610	.56	0.8931		44.44
2.	11.1	505°C	280	622.1	612.8	.5586	1.1476		44.55
3.	17.3	550°C	325	622.1	616.7	.5936	1.02163		40.90
4.	22.2	595°C	380	622.4	619.3	.64025	9.555		36.13
5.	34.71	625°C	425	622.3	622.0	.7921902	0.972		20.80
6.	44.40	675°C	525	621.7	622.31	.777	.9455128		22.22
7.	59.40	700°C	572	621	622.4	.8162	.86844		18.28

the advantage of calculating the specific cutting energy theoretically for different cutting environment is not available for Titanium.

It is observed that forces reduction during cutting mild steel at low temperature is accompanied by an increase in shear angle. If shear plane theory is applied to the Titanium it can be seen from Table 3.10 that considerable increase in shear plane angle occurs when cutting Titanium at low temperature. But at the same time there is negligible increase in cutting force  $F_c$ . It can be concluded that either the mechanism of chip formation of Titanium is different than that with continuous chips formation or shear angle adjustment cannot be a means for improving the machinability of Titanium.

### 3.2.3 Improvement in Wear

Greatest difficulty encountered in cutting Titanium was the generation of very high cutting temperature, which led to higher tool wear and poor surface finish. This is the main reason why Titanium and its alloys are cut at lower cutting speed (60 m/min), which hamper the productivity of industry. During the experiments it was observed that this metal could be cut at sufficiently high speed when liquid nitrogen was used. Also there is no significant change in forces it can be assumed roughly that wear is only temperature dependent.

From Figure 3.12 and Fig. 3.13 it can be seen that, particular temperature is reached at lower speed in case of dry cutting whereas it is attained at much higher speed when cutting

is done under liquid nitrogen environment. It is possible to calculate the percentage gain in the velocity for same interface temperature. Computing the values of the two velocity for same interface temperature from figures (3.12) and (3.13), a quantity  $\Delta V$  is obtained. A Gain Factor G can be calculated as

$$G = \frac{\Delta V}{V_1} \times 100$$

the quantity G would represent the possible rise in cutting velocity when machining with liquid nitrogen for same interface temperature. Calculated values of G for various speeds have been plotted in Fig. 3.17. As can be seen from the figure the Gain Factor is higher for lower feed.

The possible reason for the increase in gain factor may be due to less heat generation in lower feed for same quantity of  $LN_2$  supply at the same speed.

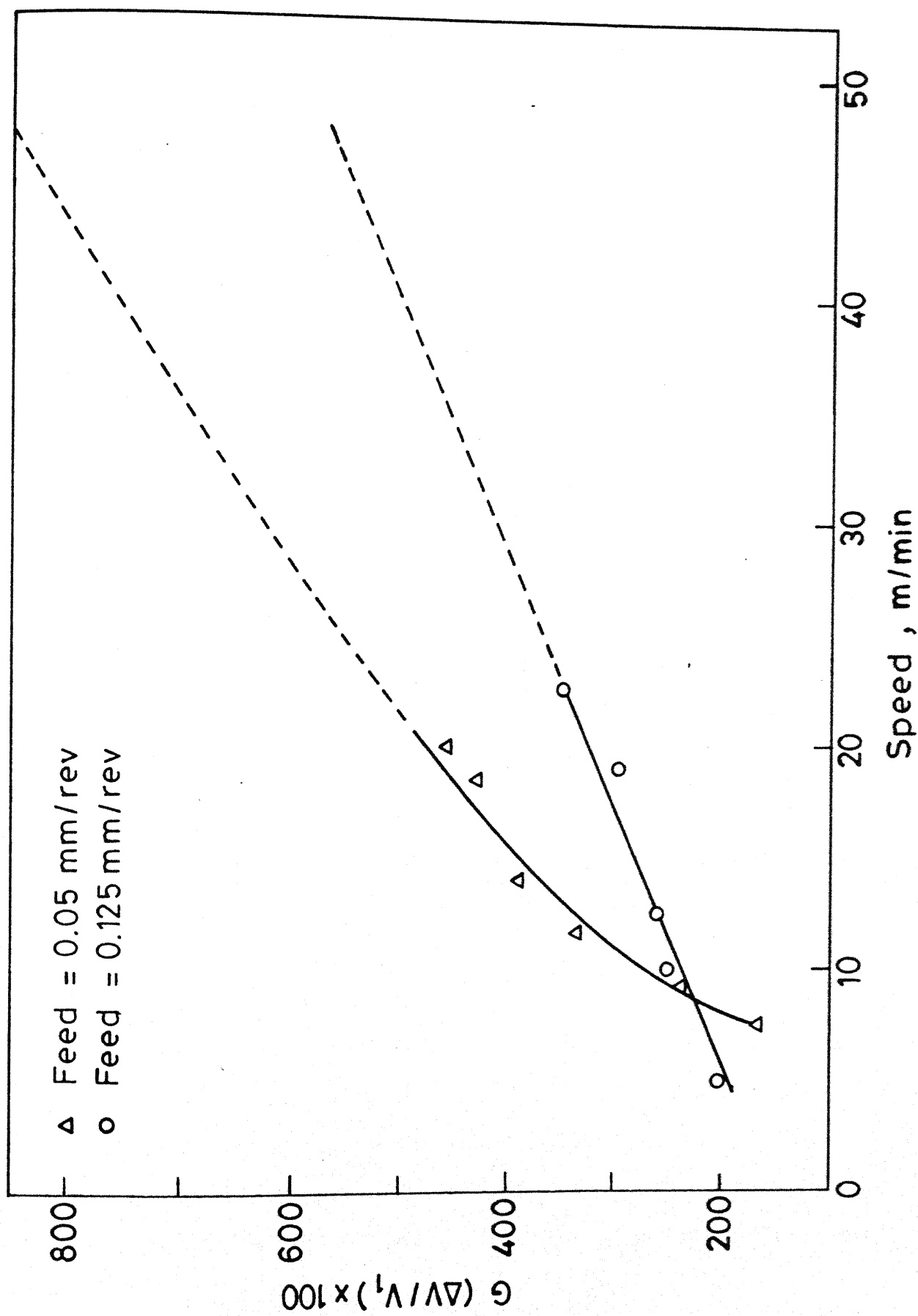


Fig.3.17 Variation of percentage gain factor  $G$  with speed (experimental) for Ti

- (8) Mechanism of chip formation at low temperature does not change for mild steel.
- (9) A wide increase in cutting range can be achieved when machining Titanium for same tool wear, hence productivity can be increased drastically.

#### 4.2 Scope of Further Research

In high strength, heat resistant metal and alloys heat generation, as well as cutting force are much more. Conventional coolants fail to remove the heat generated in machining and may **effect** adversely tool life. In much of the case machining operation are done at low cutting speeds. Using liquid nitrogen as a cooling agent above problem can be avoided and productivity can be enhanced by working at higher speeds.

As liquid nitrogen cost much more than the conventional coolants so economic of the process should be work out to optimize the use of liquid Nitrogen as coolants.

# REFERENCES

1. M.F. Ashby, "A First Report on Deformation-Mechanism Maps", *Acta Metallurgica*, Vol. 20, July 1972, p. 887.
2. 'Advance in Cryogenic Engineering', Vol. 13, ed by Timmerhans, Plenum Press, New York.
3. DT Read and RP Reed, Fracture and Strength Properties of Selected Austenitic Stainless Steels at Cryogenic Temperatures, *Cryogenics*, July 1981, p. 451.
4. H.M. Rosenberg, 'Low Temperature Solid State Physics, Clarendon Press, Oxford.
5. Materials at Low Temperatures, edited by Richard P. Reed and F. Clark, American Society for Metals.
6. Shaw, M.C., 'Metal Cutting Principles' Clarendon Press, Oxford.
7. 'Machining the space age metals' Technical Publication committee American Society of Tool and manufacturing Engg., Dearborn, Michigan 1965.
8. Hellies, W.S., "The Application and Effect of Controlled Atmosphere in the Machining of Metals, *Inst. J. Mech. Tool, Des. Res.*, September, 1961.
9. 'Refrigerated Cutting Tool Improve Machining of Supper Alloys,' *Annon Cutting Tool Engg.*, Vol. 25, No. 11-12, Nov.-Dec. 1973, pp. 12-14.
10. Cold Machining High Density Tungsten, *Cutting Tool Engg.*, Vol. 22, No. 5, May 1970, pp. 11-13.
11. S.N. Filoneko and P.T. Sibodyanik, 'Chip Deformation and Surface Finish when Turning in Tractable Materials at Low Temperature, *Machinos and Tooling*, Vol. 46, No. 2, 1975, pp. 42-44.
12. Uhera, K. and Kumagai, S., Chip Formation, Surface Roughness Cutting Forces and Tool Wear in Cryogenic Machining, *Annals, CIRP*, 1968, 17(10).
13. Uhera, K. and Kumagai, S., Mechanics of Tool Wear, *J. JSPE* 1965, 35 (9).
14. Fillippi, A.D. and Ippolito, R., Face Milling at 180°C *Annals CIRP*, 1970, 19(1).

15. Chattopadhyay, A.B., Roy, T.K. and Bhattacharya, A., Application of Cryogenics in Metal Cutting, J. Inst. of Engg. (India), 1972.
16. Yamaya, S. Shibuki, K. and Ansai, N., Study of Alumina Carbide Tools, Yung Alloy, April 1974, 19(26).
- 17.
18. Chattopadhyay, A.B. and Bajranglal, J.R., Role of Cryogenics in Metal Cutting Industry, Proc. 2nd NSC Sym., Delhi, 1981.
19. 'Austenization of Steel during Chip Formation', University of Birmingham, Metal Trans., V-14, No. 8, Aug. 1983, pp. 1743-45.
20. Pathak Ajit Kumar, An Experimental Investigation into Low Temperature Machining of Some Engineering Materials, M. Tech. Thesis, Mechanical Engineering Department, IIT Kanpur, 1986.
21. "Machining Difficult Alloys", sponsored by US Air Force, The American Society for Metals, 1962.
22. Komanduri, R., Some Clarification on the Mechanics of Chip Formation when Machining Titanium Alloys, Wear, 76 (1982), pp. 15-34.
23. 'Catastrophic Thermoplastic Shear', R.F. Recht Trans. ASME (J. App. Mech) Vol. 32, p. 189 (1964).
24. "The Formation of 'Saw-Toothed' Chips in Metal Cutting, K. Nakayama, Proc. Int. Conf. Prod. Eng., p. 572 (1974).
25. R. Komanduri and B.F. Von Turkovich, 'New Observation of the Mechanical of Chip Formation when Machining Titanium Alloys, Wear, Vol. 69, p. 179 (1981).
26. The Split Shear Zone Mechanism of Chip Segmentation, C.A. Van Luttervalt, Annals of CIRP, Vol. 25/1, p. 33, 1977.
27. Brow, C.J. and B.K. Hinds, Forces and Temperature Effects with Machining Titanium", Proc. of North American Manufacturing Society, 1985.
28. Boothroy Geoffrey, Fundamental of Metal Machining and Machine Tools, McGraw Hill, Kogakusha, Ltd., 1975.



